# PREPARATION AND CHARACTERIZATION OF PLATINUM/CARBON CATALYSTS SYNTHESIZED BY DIFFERENT REDUCING AGENTS AND SURFACTANTS AND THEIR PERFORMANCE TOWARDS METHANOL OXIDATION REACTION

A THESIS SUBMITTED TO
THE GRADUATE SCHOOL OF NATURAL AND APPLIED SCIENCES
OF
MIDDLE EAST TECHNICAL UNIVERSITY

BY

DENİZ ÇAKAL

IN PARTIAL FULFILLMENT OF THE REQUIREMENTS
FOR
THE DEGREE OF MASTER OF SCIENCE
IN
CHEMISTRY

JUNE 2014

Approval of the thesis:

**PREPARATION AND CHARACTERIZATION OF PLATINUM/CARBON CATALYSTS SYNTHESIZED BY DIFFERENT REDUCING AGENTS AND SURFACTANTS AND THEIR PERFORMANCE TOWARDS METHANOL OXIDATION REACTION**

submitted by **DENİZ ÇAKAL** in parial fulfillment of the requirements for the degree of **Master of Science in Chemistry Department, Middle East Technical University**by,

Prof. Dr. Canan Özgen
Dean, Graduate School of **Natural and Applied Sciences** _____

Prof. Dr. İlker Özkan
Head of Department, **Chemistry** _____

Prof. Dr. Gülsün Gökağaç
Supervisor, **Chemistry Dept., METU** _____

**Examining Committee Members:**

Prof. Dr. İnci Eroğlu
Chemical Engineering Dept., METU _____

Prof. Dr. Gülsün Gökağaç
Chemistry Dept., METU _____

Prof. Dr. Ceyhan Kayran
Chemistry Dept., METU _____

Assoc. Prof. Dr. Ayşen Yılmaz
Chemistry Dept., METU _____

Assoc. Prof. Dr. Emren Nalbant Esentürk
Chemistry Dept., METU _____

Date: **03.06.2014**

**I hereby declare that all information in this document has been obtained and presented in accordance with academic rules and ethical conduct. I also declare that, as required by these rules and conduct, I have fully cited and referenced all materials and results that are not original to this work.**

Name, Last name: Deniz Çakal

Signature:

## ABSTRACT

PREPARATION AND CHARACTERIZATION OF PLATINUM/CARBON CATALYSTS SYNTHESIZED BY DIFFERENT REDUCING AGENTS AND SURFACTANTS AND THEIR PERFORMANCE TOWARDS METHANOL OXIDATION REACTION

Çakal, Deniz
M.S., Department of Chemistry
Supervisor: Prof. Dr. Gülsün Gökağaç

June 2014, 64 pages

In this thesis, platinum nanoparticles were prepared by using $PtCl_4$ as a starting material, sodium borohydride (Group I), hydrazine (Group II) and formaldehyde (Group III) as reducing agents and hexylamine (Group -a), N-methylhexylamine (Group -b), N,N-dimethylhexylamine (Group -c) as surfactants (the last two surfactants were used for the first time). These platinum nanoparticles were dispersed on Carbon XC-72 to be utilized as catalyst for methanol oxidation reaction which can be used in direct methanol fuel cells. The characterization, electrochemical properties and performance of catalysts were defined by using inductively coupled plasma spectroscopy (ICP), cyclic voltametry (CV), chronoamperometry (CA), X-ray diffraction (XRD), X-photoelectron Spectroscopy (XPS), transmission electron microscopy (TEM), BET surface area analysis and fourier transform infrared spectroscopy (FTIR).

XRD and TEM results indicated that platinum crystallizes in face-centered cubic (fcc) structure with a size of ~5 nm. In addition to these small particles, agglomerated particles were also observed in different size, shape and density. In Group I, cubic platinum nanoparticles come together to form large particles with a

size of 20 - 200 nm. In Group II, agglomerated particles were appeared to be dense, large and spherical lumps with a size of 50 - 200 nm. In Group III, the agglomerated particles were also formed in spherical shape but not as much dense and large (50 - 150 nm) as in Group II.

XPS results revealed that there are two different oxidation states of platinum in each catalyst. These are Pt(0) and Pt(IV) and their percentages changes between 65 - 73 and 35 - 27, respectively. XPS data also showed the existence of two kinds of oxygen, $HO_{ads}$ and $H_2O_{ads}$, with a ratio of 85:15, 90:10 and 80:20 for Group I, II and III, respectively.

BET analyses indicated that the surface area of catalysts depends on reducing agent not surfactant. It was 30 - 35 $m^2/g$, 4 - 9 $m^2/g$ and 20 - 30 $m^2/g$ for Group I, II and III, respectively.

CV records demonstrated that the order of catalysts performance was Group II < Group I < Group III. Within all catalysts, Catalyst IIIb exhibited the highest performance (258 mA/mg Pt) towards methanol oxidation reaction and provided 3.5 times greater performance than the commercial E-TEK Pt catalyst. All these data indicated that the performance of these catalysts depends on:

a) active surface area,

b) $HO_{ads}$/ $H_2O_{ads}$ ratio, and

c) morphology of the catalysts.

Keywords: Direct Methanol Fuel Cells, Carbon-Supported Platinum Nanoparticles, Transmission Electron Microscopy, X-ray Diffraction, X-ray Photoelectron Spectroscopy, Cyclic Voltammetry.

# ÖZ

FARKLI SÜRFAKTANT VE İNDİRGEYİCİ AJANLAR KULLANILARAK PLATİN/KARBON KATALİZÖRLERİN HAZIRLANMASI, KARAKTERİZASYONU VE METHANOL YÜKSELTGENME REAKSİYONUNDAKİ PERFORMANSI

Çakal, Deniz
Yüksek Lisans, Kimya Bölümü
Tez Yöneticisi: Prof. Dr. Gülsün Gökağaç

June 2014, 64 sayfa

Bu tez çalışmasında, başlangıç maddesi olarak $PtCl_4$, indirgeyici olarak sodyum borohidrat (Group I), hidrazin (Group II) ve formaldehit (Group III), sürfaktant olarak da hekzilamin (Group -a), N-metilhekzilamin (Group -b), N,N-dimetilhekzilamin (Group -c) kullanılarak platin nanoparçacıklar hazırlanmışır (son iki sürfaktant burada ilk kez kullanılmıştır). Pt nanoparçacıkların karbon üzerine dağıtılmasıyla hazırlanan katalizörler, doğrudan methanol yakıt hücresinde gerçekleşen metanol yükseltgenme tepkimesinde kullanılmıştır. Hazırlanan katalizörlerin karakterizasyonu, elektrokimyasal özellikleri ve performansları indüktif eşleşmiş plazma (ICP), dönüşümlü voltametre (CV), kronoamperometre (CA), X-ışınları kırınımı (XRD), X-ışınları fotoelektron spektroskopisi (XPS), transmisyon (geçirmeli) electron mikroskopu (TEM), BET yüzey analizi, fourier dönüşümlü kızılötesi spektrometresi (FTIR) gibi teknikler kullanılarak yapılmıştır.

XRD ve TEM sonuçları platinin ~5 nm büyüklüğünde, yüzey merkezli kübik yapıya sahip olduğunu göstermiştir. Bu küçük parçacıkların yanında değişik büyüklükte, şekilde ve yoğunlukta büyük parçacıkların da olduğunu göstermiştir. Grup I'de kübik platin nanoparçacıkları bir araya gelerek 20 - 200 nm büyüklüğünde büyük

parçacıklar oluşturmuştur. Grup II 50 - 200 nm büyüklüğünde yoğun, büyük ve yuvarlak platin parçacıklarından oluşurken, Grup III yine yuvarlak ancak daha az yoğun ve küçük (50 - 150 nm) platin parçacıklarından oluşmuştur.

XPS sonuçları platinin iki değişik oksidasyon durumunda olduğunu göstermiştir. Bunlar % 65 - 73 miktarında Pt(0) ve % 35 - 27 miktarında Pt(IV)'den oluşmaktadır. XPS verileri, $HO_{ads}$ ve $H_2O_{ads}$ olmak üzere, oksijenin de iki çeşit olduğunu göstermiştir. $HO_{ads}$:$H_2O_{ads}$ oranının Grup I, II ve III için 85:15, 90:10 ve 80:20 olduğu tespit edilmiştir.

BET analizleri katalizörlerin yüzey alanlarının sürfaktantlara değil, indirgeyicilere bağlı olduğunu göstermiştir. Grup I, II ve III için yüzey alan değerleri 30 - 35 $m^2/g$, 4 - 9 $m^2/g$ ve 20 - 30 $m^2/g$'dır.

CV grafikleri katalizörlerin performansının Grup II < Grup I < Grup III düzeninde olduğunu göstermiştir. Bütün katalizörler gözönüne alındığında ise Katalizör IIIb'nin metanol yükseltgenmesi tepkimesine karşı en aktif (258 mA/mg Pt) katalizör olduğunu göstermiştir. Bu değer ticari olarak satılan E-TEK Pt katalizörünün 3.5 katı kadardır.

Bütün bu veriler, katalizörlerin performanslarının katalizörlerin:

a) aktif yüzey alanına,

b) $HO_{ads}$/ $H_2O_{ads}$ oranına, ve

c) morfolojisine bağlı olduğunu göstermiştir.

Anahtar Kelimeler: Doğrudan Methanol Yakıt Pilleri, Karbon Destekli Platin Nanoparçacıklar, Transmisyon Electron Mikroskobu, X-ışınları Kırınımı, X-ışınları Fotoelektron Spektroskopisi, Dönüşümlü Voltametre.

To my parents…

## ACKNOWLEDGEMENTS

Firstly, I would like to express my sincere appreciation and thanks to my supervisor Prof. Dr. Gülsün Gökağaç for her guidance, encouragement, support and valuable ideas throughout the research.

I would like to thank Assoc. Prof. Dr. Ayşen Yılmaz for her help during XRD measurement.

I want to thank Dr. Fatih Şen for his advices during Master study.

I would like to thank Güzide Aykent for her endless support.

I want to thank my lab-mates Aysu Aslantürk, Sevda Kalyoncu, Seda Ergan for providing enjoyful working environment.

I wish to express my special thanks to my dearest friends Başak Çikot, Gizem Tanrıvere, Melek Mutioğlu for their real friendship and moral support and understanding.

I would like to thank my dear roommates Seray Akça, Reyhan Yaka, Cemile Kılıç, Shahrzad Nikghadam, Ceren Bilgen, Sema Zabcı, Hande Öztürk.

I want to thank TÜBİTAK for financial support and METU Central Lab. for measurements.

## TABLE OF CONTENTS

## LIST OF TABLES

**TABLES**

## LIST OF FIGURES

**FIGURES**

# CHAPTER 1

# INTRODUCTION

## 1.1. FUEL CELLS

Fuel cell can be defined as a device in which the chemical energy of reactants or fuels is directly converted into electrical energy. Fuel cells attract attention as an alternative to the other energy conversion Technologies such as batteries and heat engines. The comparison of fuel cells with batteries and heat engines proves the superior advantages over conventional power generation sources [1,2].

A fuel cell can steadily produce power so long as the fuel and oxidant are replenished and the reaction products are eliminated continuosly [3]. Unlike fuel cells, the batteries store a certain amount of fuel and oxidant with in a closed system and power generation ceases when the reactants within the cell are used up. Additionally, the electrodes within fuel cells are considerably stable and nonconsumable, therefore fuel cells have unlimited operation life time in principle. On the other hand, the electrodes of batteries participate in reaction and are consumed during the energy conversion process, thus the running time of batteries is limited to lifetime of electrodes [1].

A heat engine also converts the free energy of chemical substances into electrical energy as well as fuel cells. For both heat engines and fuel cells, the reactants are supplied from the outside [1]. However, the electrical energy generation in fuel cells is based on oxidation reduction reactions as distinct from heat engines in which the

electrical energy is produced from combustion reaction. Furthermore, while heat engines utilize additional energy conversion steps for power generation, fuel cells produces electrical energy directly in a one step process [1]. Therefore, the efficiency of a heat engine is rather low due to energy losses in intermediate energy conversion steps involving thermal and mechanical energy forms [1,3].

At present, the energy need of modern life is mostly fulfilled by heat engines utilizing combustion of natural resources. The utilization of these resources for large scale energy production leads to emission of pollutant gases such as $SO_x$, $NO_x$, $CO_2$ and CO, thus causing negative effects on environment and human life. Additionally, the dramatic decline in fossil fuel reserves along with industrial developments and human population growth leads to international tensions and high level of inflation. These undesirable consequences of fossil fuel consumption in the world direct the focus of research and development toward alternative energy technologies to suppy extraordinary energy requirement of world. At this point, fuel cells are receiving considerable attention as one of the most promising energy conversion devices to meet growing energy demand of modern life and lessen the negative effects of fossil fuel consumption on environment. Fuel cell as a sustainable technology offers numerous advantages over conventional power generation system [1,4]. The advantages can be given as

- Fuel cells have high energy conversion efficiency since they are not restricted by Carnot cycle efficiency [1].
- Fuel cells can be designed at any intended size to supply power a wristwatch or a large city [3].
- Fuel cells are environmentally friendly devices due to extremely low or zero emission of pollutants and particulates [1].
- Fuel cells have little or no maintenance problems and are reliable since they have no mechanical moving components [2].

- Fuel cells can prevent being dependent on limited and diminishing fossil fuel reserves, therefore eliminate economic dependence on other nations due to compatibility of fuel cells with renewable energy sources [1].
- Fuel cells can operate silently without any vibration or noise because they have few or no moving parts [2].
- Fuel cells do not suffer from "memory effect" when they are refueled [5].

Although fuel cells have numerous advantagoues characteristics, there are still some limitations of this technology. These can be given as

- Fuel cells can need expensive catalysts such as platinum and ruthenium.
- Fuelling of some fuel cells is challenging due to production, transportation, distribution and storage problems of fuels such as hydrogen.
- Fuel cell vehicles have longer refueling and starting time and shorter driving range as compared to normal car.
- Fuel cells are expensive to manufacture, since materials utilized for cell construction are expensive [6].

## 1.2. THE HISTORY OF FUEL CELLS

In 1791, a remarkable experiment performed by Italian physiologist Luigi Galvani revealed that muscle contraction occurs, similar to that produced by discharge of Leyden jar, by the contact of unlike two metals to the exposed nerve of frog. In 1792, this phenomenon was correctly interpreted by Italian physicist Alessandro Volta. According to him, this galvanic effect arises from the contacts between these two metals and between these two and the muscle tissue. On the basis of this idea, in 1800, Volta constructed first simple electrochemical device known as Volta pile, which could generate "inexhaustable electric charge" by contact of unlike metals. With the construction of *Volta pile*, crucial developments were succeeded in fields of electricity and electrochemistry since continous electric current could now be

achievable. In a short time, the charateristics and effects of electric current involving numerous electrochemical processes were detected [3].

In the light of these developments, British scientists William Nicholson and Sir Anthony Carlisle achieved to produce hydrogen and oxygen from water by electrolysis process in May 1801. In the 1830s, not only a trained lawyer and but also an amatuer scientist Sir William Robert Grove performed a series of experiments on electrolysis of water in a cell containing two platinum electrodes submerged into aqueous sulfuric acid solution as illustrated in Figure 1.1. He thought that if the water can be decomposed into hydrogen and oxygen depending on the applied current, the reverse reaction should be possible by consumption of hydrogen and oxygen at the same electrodes with generation of electric current. He noticed that platinum electrodes were polarized after stopping the flow of current, in other words, a certain potential difference was retained between the electrodes. As a following step, these electrodes were externally linked with a circuit and the current was realized to pass through this circuit. This invention was called as *gas voltaic battery* by Grove and accepted as the first unmistakable illustration of fuel cell principle. In 1839, the experimantal results of Grove were published in the *Philosophical Magazine* [3,7].

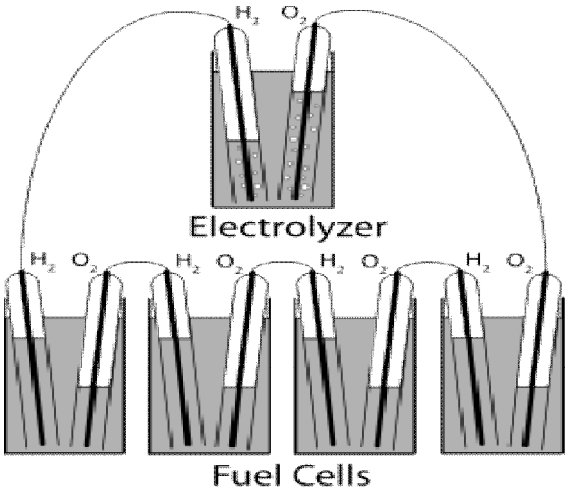


**Figure1.1.** A schematic representation of Grove's gas battery [8].

In 1882, “a new form of gas battery” was introduced by the British Physicist Lord Rayleigh. He provided the enhancement of electrode efficiency by increasing the contact area of solid Pt electrodes with gases and electrolyte. He also used coal gas as fuel for the first time [9].

The another new form of gas battery was offered in 1889 by Ludwig Mond and Carl Langer. This new form of gas battery was regarded as the first technical fuel cell in which sulfuric acid was held in a porous, non-conducting solid material instead of being free liquid to prevent electrode flooding with electrolyte. In fuel cell of Mond and Langer, thin and perforated platinum electrodes with large specific surface area were used to yield larger currents [3,9].

In 1894, German scientist Wilhelm Oswald, the father of physical chemistry, came up with the offer to construct devices for oxidation of natural fuels with air by direct electrochemical processes without generation of heat. He thought that using electrochemistry would be a solution to low energy conversion efficiency of steam engines since only 10% of chemical energy of coal was transformed into mechanical energy during combustion due to thermodynamic limitations. However, Oswald’s idea remained in theory, since constructing a device for direct electrooxidation of natural fuels was quite difficult. His approach only provided the theoretical comprehension of how fuel cells operate [9].

In 1896, William Jacques reported to have develop a fuel cell generating electricity directly from coal. However, in 1904, Haber and Bruner realized that the anodic reaction in *Jacques cell* was actually oxidation of hydrogen produced by touch of iron with water in the electrolyte instead of direct oxidation of coal [3]. After this discovery, Haber and Bruner attended to study on direct coal fuel cells. Subsequent research on direct coal fuel cells was done by Baur and Ehrenberg in 1912. They tested various types of electrolytes containing silicate, carbonate, hydroxide and borate to select suitable one after detecting molten silver as proper cathode [9].

After the study of Baur and Ehrenberg, Baur and Brunner' research focused on improvement of fuel cell. They realized that performance of fuel cell was enhanced when $CO_2$ was supplied to cathode. They also pointed out that the electrolytes in molten state resulted in large difficulties in fuel cell operation due to the electrode flooding problem. Therefore, they deduced that a solid electrolyte would be more convenient for operation and focused on their investigation on ceramic materials for this purpose [9].

In 1930s, the Armenian scientist Oganes Davtyan performed studies to improve the conductivity, chemical stability and mechanical strength of electrolytes. For this purpose, he prepared a electrolyte mixture containing monozite sand, tungsten trioxide, sodium carbonate, quartz and clay. He also conducted many studies on low temperaure and high temperature fuel cells. His studies was presented in a book published in 1947 [3,9].

In 1932, an engineer Professor Francis Thomos Bacon started to work on modification of Mond-Langer battery with an engineer approach. He designed the first alkaline fuel cell by replacing corrosive acidic solution with alkaline KOH solution. He also used nickel powdered electrodes treated with hot lithium hydroxide solution to lower corrosion risk. His cell design was patented as *Bacon cell* in 1959. In 1960, Bacon's cell was demostrated in public and received significant attention from many scientists. Just after the demonstration, the work of Grubb and Niedrach (1960), and Grubb and Michalske (1964) revealed for the first time that electrochemical oxidation of hydrocarbons such as methane, ethane and ethylene was feasible by using platinum electrodes under 150 ºC [3].

In the second half of 1900s, the fuel cells was developed to be utilized for commercial applications. A new agency in the United States, the National Aeronautics and Space Administration (NASA), colloborated with industrial partners to make the fuel cell technology appliciable for manned space missions. In 1955, Thomas Grubb and Leonard Niedrach working for the General Electric Company

(GE) developed a fuel cell by using Proton Exchange Membrane (PEM) as the electrolyte. This design named as *Grubb-Niedrach fuel cell* was further developed by NASA and used for *Gemini* space project. This was the first commercial use of fuel cells. However, when *Gemini* flight mission ended, the use of PEM was ceased [3].

In the early 1960s, Pratt & Whitney Aircraft company took a license of Bacon's patent and modified Bacon's design by lowering the weight and increasing KOH concentration. This improved alkaline fuel cell provided longer duration and higher effficiency as compared to GE PEM design. Consequently, Pratt & Whitney gained a contract from NASA and these fuel cells were utilized in *Apollo* program for space flight mission. Alkaline fuel cells have also been used for subsequent space missions in the U.S. [3].

In the 1970s, fuel cell technology was started to be used for systems on Earth as well as space missions. The oil embargo in 1973 functioned as a trigger for arising research interest of fuel cells in terrestrial applications. As a result, goverment organizations, companies and researchers spent immense effort to commercialize fuel cell vehicles. During 1970s and 1980s, therefore, the research interest was focused on developing the materials for fuel cell systems, determining optimum fuel sources and lowering the high cost of this technology. In the 1980s, fuel cells were again regarded as power supply for transportation vehicles. In 1993, the first fuel cell-powered transportion vehicle was manufactured by the Canadian company Ballard Power Systems. In the 2000s, the fuel cells continued to be developed with a rising interest for many different applications as can be seen in following section [9].

## 1.3. THE APPLICATION OF FUEL CELLS

Fuel cell systems can generate power for a wide range of applications. These applications can be divided into three main categories as stationary power generation, transportation and portable applications. Fuel cells can be used in hospitals, apartment houses, electric utility industries and office buildings as stationary power source with several hundered kW cogeneration, in transportation

vehicles such as automobiles, buses and bicycles as several kW power generation source and in portable devices such as mobile phones, movie cameras, notebook computers as several 10 W power generation source [1,3,9].

## 1.4. THE TYPES OF FUEL CELLS

Fuel cells can be classified according to a variety of different criteria such as the type of electrolyte, the type of primary fuels and oxidants, direct or indirect use of primary fuels and operating temperature and so on. Here the type of electrolyte is used as to classify the fuel cells, and it is found that there are five different types of fuel cells. These are polymer electrolyte membrane (PEM), alkaline fuel cell (AFC), phosphoric acid fuel cell (PAFC), molten carbonate fuel cell (MCFC), solid oxide fuel cell (SOFC). The operational properties, applications and advantages of these fuel cells are given in Table 1.1. [5].

**Table 1.1** The operational properties, applications and advantages of fuel cells [5].

| Fuel Cell Type | Common Electrolyte | Operating Temperature | Electrical Efficiency | Combined Heat and Power Efficiency (CHP) | Applications | Advantages |
|---|---|---|---|---|---|---|
| **Polymer Electroyte Membrane(PEM)**<br>----------<br>***Direct Methanol (DMFC)** | Solid organic polymer Poly-perfluorosulfonic acid | 50 - 100 ºC<br><br>60 – 90 ºC | 53- 58 % (transportation) 25- 35 % (stationary)<br><br>20- 25 % | 70-90 % (low grade waste heat ) | -Backup power<br>-Portable power<br>-Small distributed generation<br>-Transportation<br><br>-Mobile | -Solid electrolyte reduces corrosion & electrolyte management problems<br>-Low temperature<br>-Quick start-up<br><br>-No reforming needed<br>-Easy storage and transport |
| **Alkaline (AFC)** | Aqueous solution of potassium hydroxide soaked in a matrix | 90-100 ºC | 60 % | > 80 % (low grade waste heat ) | -Military<br>-Space | -Cathode reaction faster in alkaline electrolyte leads to higher performance<br>-Can use a variety of catalysts |
| **Phosphoric Acid (PAFC)** | Liquid sulfuric acid soaked in a matrix | 150-200 ºC | > 40 % | > 85 % | -Distributed generation | -Higher overall efficiency with CHP<br>-Increased tolerance to impurities in hydrogen |
| **Molten Carbonate (MCFC)** | Liquid solution of lithium, sodium and/or potassium carbonates soaked in a matrix | 600-700 ºC | 45- 47 % | > 80 % | -Electiric utility<br>-Large distributed generation | -High efficiency<br>-Fuel flexibility<br>-Can use a variety of catalysts<br>-Suitable for CHP |
| **Solid Oxide (SOFC)** | Yttria<br>stabilized zirconia | 600-1000 ºC | 35- 43 % | < 90 % | -Auxiliary power<br>-Electiric utility<br>-Large distributed generation | -High efficiency<br>-Fuel flexibility<br>-Can use a variety of catalysts<br>-Suitable for CHP<br>-Solid electrolyte reduces electrolyte management problems |

*Direct Methanol Fuel Cell is a subcategory of PEM fuel cell.

## 1.5. DIRECT METHANOL FUEL CELL

In the last decade, it is greatly desirable to use organic liquid fuels such as alcohols or hydrocarbons for fuel cell applications due to their easy transportation and storage. Methanol is a good choice of fuel among other organic liquids in terms of high energy density (~20 MJ/kg), reactivity at low temperatures, availability, handling, refuelling, storage and absence of pollutants except for $CO_2$. These advantageous properties of methanol makes direct methanol fuel cells (DMFCs) specifically significant for applications in mobile power plants and more specifically, small fuel cells as power supply to portable electronic devices such as mobile phones, notebook computers. Moreover, high energy density of methanol as compared to other organic liquids and petroleum products makes DMFC application available for large power plants in electric vehicles [1,3].

Direct methanol fuel cells consist of two electrodes at which electrochemical oxidation and reduction reactions take place. These reactions are mostly carried out in acidic electrolytes to provide carbon dioxide rejection without formation of insoluble carbonates which occur in alkaline electrolytes. The components of a DMFC is schematically illustrated in Figure 1.3. As it can be seen from the figure, methanol is electrochemically oxidized to carbon dioxide at the anode while oxygen is reduced to water at the cathode. The current generation is provided by transport of the electrons given off in anode half reaction into cathode through an external circuit. The circuit is maintained by the transport of protons to cathode through the electrolyte membrane [3,7]. The reactions occuring at the anode and cathode and overall reaction are summarize below:

Anode half reaction:

$$CH_3OH + H_2O \rightarrow 6\,H^+ + 6\,e^- + CO_2 \qquad E^0 = 0.02\ V$$

Cathode half reaction:

$3/2\ O_2 + 6\ H^+ + 6\ e^- \rightarrow 3H_2O$ $\qquad E^0 = 1.23$ V

Overall reaction:

$CH_3OH + 3/2\ O_2 \rightarrow CO_2 + 2H_2O$ $\qquad E^0 = 1.21$ V

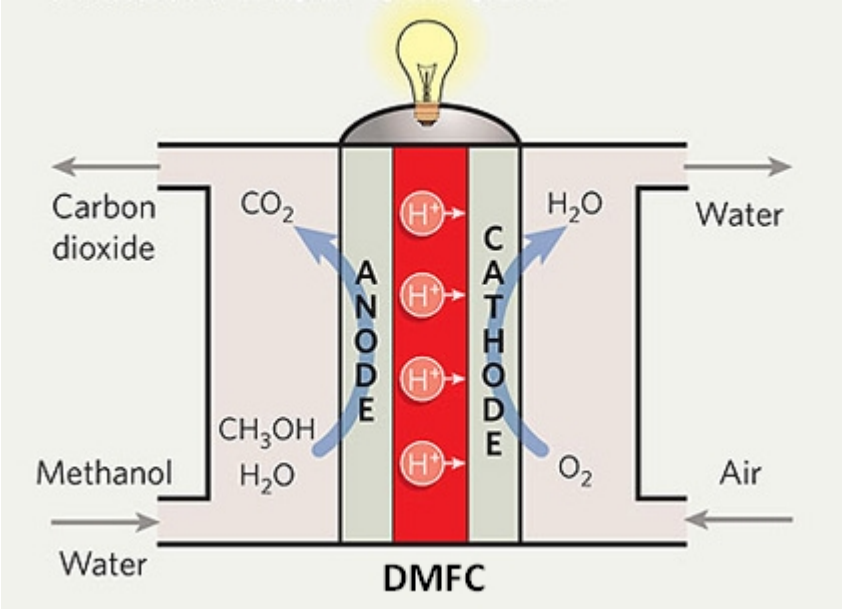


**Figure 1.2.** Schematic representation of a DMFC with acidic solid polymer electrolyte [5].

Although the major product in overall cell reaction is carbon dioxide, some other by-products such as formaldehyde, formic acid, bridged or linearly bonded CO occur on the surface of catalyst. Indeed, methanol oxidation reaction does not take place in a single step. The actual electrooxidation mechanism consists of several consequtive stages. At first stage, methanol is adsorbed on the surface of catalyst for dehydrogenation to chemisorbed species $COH_{ads}$ as follow:

$CH_3OH \rightarrow COH_{ads} + 3\ H^+ + 3\ e^-$

At the subsequent stage, these dehydrogenated species, $COH_{ads}$ are oxidized with the oxygen containing species, $H_2O_{ads}$ or $OH_{ads}$ coadsorbed on neighboring sites of catalyst to produce carbon dioxide which desorbs from catalyst surface as follow:

$$COH_{ads} + H_2O_{ads} \text{ ( or } OH_{ads}) \rightarrow CO_2 + 3\,H^+ + 3\,e^-$$

Under certain circumstances, $H_2O_{ads}$ or $OH_{ads}$ species may not be adsorbed on the surface of catalyst therefore, $COH_{ads}$ species age and turn into $CO_{ads}$ species. These species result in poisioning on the surface of catalyst and further electrosorption of methanol cannot occur until the adsorbed $CO_{ads}$ species oxidized to carbon dioxide. In Figure 1.3., methanol adsorption mechanism and poisioning formation on the surface of platinum catalyst are schematically represented [3,7].

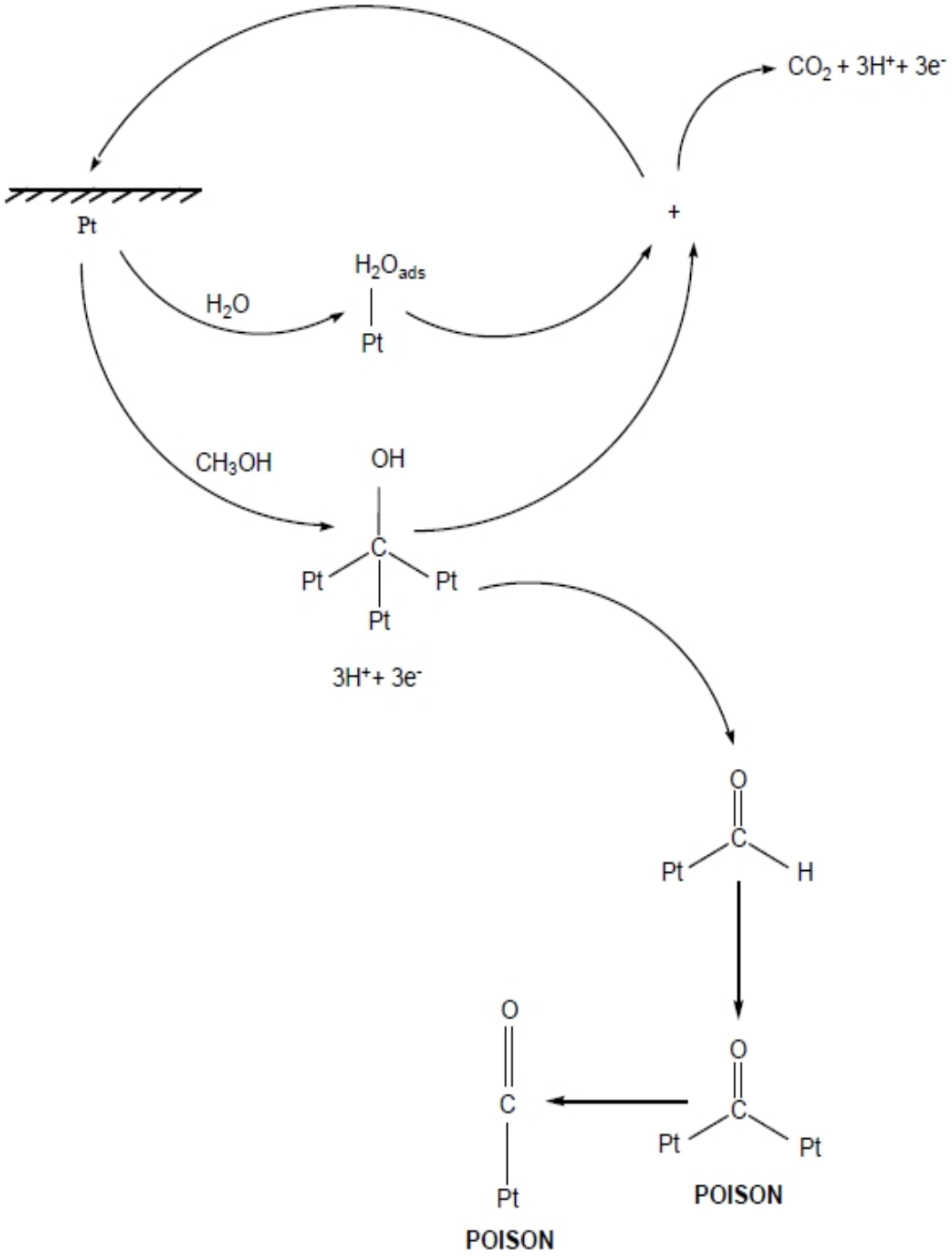


**Figure 1.3.** Methanol electrooxidation mechanism and poisoning on pure Pt surface in acid electrolyte [10].

## 1.6. THE NEED FOR CATALYST

The major limitation of employing methanol in fuel cells is the poor electrochemical performance of methanol in acidic medium at low potentials. In order to activate the methanol used in fuel cells, efficient catalyst materials are needed. After the great research effort spent for investigation and identification of proper catalyst material, it was found that only platinum-based catalysts specifically platinum itself provide the resonable activity and good stability required for activation of methanol. After that, research focus has been centered on enhancement of activity of Pt-based catalyst materials [7,11]. The studies conducted for this purpose demonstrated that high catalytic activity is generally achieved by increasing the active surface area of the catalyst by reducing size of particles in catalyst material. At this point, nanotechnology provides the key solution for preparation of highly efficient catalyst materials [1,12].

## 1.7. LITERATURE SURVEY OF NANOPARTICLES RELATED WITH THIS STUDY

Nanoparticles can be defined as ultrafine particles with the size ranging from 1 nm to 100 nm. Nanoparticle research is recently the most studied branch of science with the potential use of nanoparticles for numerous applications such as biomedical, electronic, energy, magnetic and optical fields. Nanoparticles are receiving great attraction since they provide the connection between the bulk materials and atomic or molecular structures. The bulk materials have certain physical and chemical properties without being dependent upon the size of material. However, the nano-sized particles of the same material may exhibit different properties from the bulk material depending on its size and shape. This difference can be attributed to the change in bonding state of atoms and molecules involved in nanoparticle. As the size of material approaches the nanoscale, the ratio of surface to bulk atoms increases which create large surface area to achieve chemical reaction on heterogeneous catalysts [13,14]. Metal nanoparticles are extensively used for this purpose in fuel

cell technology and Pt is the most commonly used catalyst material in this field. However, the performance of Pt-based nanoparticle catalysts is remarkably based on preparation methods and conditions, supporting materials and the nature of additives [15,16]. Much research effort has therefore centered on preparation of Pt nanocatalysts to enhance their performance. One approach is to select proper support material for enhancing utilization efficiency of Pt nanoparticles. In this context, carbon materials have emerged as the most important catalyst support material for fuel cells since they hold a great potential in constructing high performance Pt catalysts owing to their large surface area and superior electrical conductivity. There are many types of carbon materials used as support such as Vulcan XC-72 carbon black, carbon nanotubes, carbon nanofibers and mesoporous carbons. XC-72 carbon black is the most preferred carbon support material for preparation of fuel cell catalyst [15,17-19]. Another effective approach for increasing the activiy of Pt-based catalysts is to incorporate a second or third metal such as Ru, Pd, Sn, Rh and Ni as promoter to create much effective Pt-based catalysts [18,20,21]. Among the Pt alloy catalysts, PtRu system is the most active bimetallic catalyst and there are numerous studies on this type of catalyst in literature. Recently, Liu et al. prepared carbon-supported Pt and PtRu catalysts by using microwave-assisted polyol method and showed that binary catalyst exhibits better electrochemical performance than only Pt catalyst towards methanol oxidation reaction [22]. In another study, Şen et al. prepared carbon-supported PtRu binary catalysts with simultaneous reduction of Pt and Ru ions in the presence of superhydride. These carbon-supported PtRu bimetallic catalysts revealed much better catalytic performance than the corresponding monometallic Pt catalyst for both methanol and ethanol oxidation reactions. The performance of these binary catalysts also showed improved results compared to that of commercial E-TEK Pt/C and PtRu/C catalysts [23]. Öztürk et al. also prepared binary catalytsts by inserting different percentages of Pd in Pt nanoparticles with simultaneous reduction of these metal salts by superhydride in the presence of two different surfactants, hexanethiol and 1,1-dimethylhexanethiol. It was found that 1,1-dimethylhexanethiol stabilized PtPd/C catalyst with 12% of Pd loading exhibited 1.7 and 1.8 times higher performance than Pt/C catalyst for methanol and ethanol

oxidation reactions, respectively. It was also reported that the performance of this PtPd alloy catalyst is 5.0 and 14.0 times higher than commercial Pt E-TEK catalyst for methanol and ethanol oxidation reactions, respectively [20]

As another approach, preparation methods and conditions should be taken into consideration for obtaining high performance Pt catalysts in fuel cell applications. It is well known that the performance of fuel cell catalysts are strongly dependent on the size and shape of prepared Pt nanoparticles and their dispersion on support material. In order to produce Pt nanoparticles at intended size and shape, it is crucial to choose the appropriate preparation route and control the parameters in the course of preparation. The most preferred route used for preparation of supported and unsupported Pt nanocatalyst and its alloys is the liquid phase reduction of metallic salts since such a method provides the controlled synthesis of Pt nanoparticles. The reduction is carried out by using the reducing agents such as hydrogen gas, sodium borohydride, hydrazine, formaldehyde, formic acid and so on [12,24,25]. The reducing agent is one of the important parameters influencing the size and the activity of prepared catalyst. A stronger reducing agent results in the formation of large number of nuclei with smaller size, which then continue to grow until the particle reach a critical size. The relative rates of nucleation and growth processes determines the final sizes of nanoparticles [25]. However, the reducing agent is not the only factor influencing the final size and shape of resulting nanoparticles, the use of stabilizing agent in reduction has also a significant impact on particle growth process which strongly influence the size and shape of Pt nanoparticles. There are a number of stabilizing agents used for controlled synthesis of nanoparticles, such as surfactants, polymers or ligands during reduction [12]. For example, Ertan et al. prepared carbon-supported Pt nanoparticles by using liquid-phase superhydride reduction in the presence of different surfactants and found that chain length of surfactant directly affect the size and the activity of metal nanoparticles [26]. In another study, Yang et al. reported that Pt nanoparticles stabilized with different kind of surfactants display different catalytic activity owing to the binding strength of

surfactants although the size of nanoparticles are the same [27]. There also some other parameters affecting the size, shape and correspondingly catalytic activity of Pt nanoparticles, such as use of different solvents, the nature of additives in solution, reduction temperature and the concentration of reducing agents and stabilizers. However, it is difficult to explain the exact effect of these parameters on Pt nanoparticle size and morphology since these parameters are interrelated and system dependent [28]. In this perspective, it is resonable to give more recent studies from literature. For example, Castro et al. prepared docenathiol-stabilized Pt nanoparticles by using two-phase liquid-liquid reduction method with sodium borohydride, in which freshly formed Pt nanoparticles were transferred from aqueous phase to organic phase with the help of thiol surfactant. It has been found that the addition order of reagents directly influences the formation of Pt nanoparticles in this method and the addition time of surfactant leads to different size of Pt nanoparticles and correspondingly different catalytic performance towards methanol oxidation reaction. The low catalytic activity of small-sized Pt nanoparticles can be explained by formation of more stable complex between platinum and docedanethiol owing to the immediate addition of surfactant after reducing agent [29]. A similar type of preparation route was also pursued by Yang et al. to investigate the effect of type of surfactant molecules on catalytic activity as reported above [27]. There are also different preparation routes for obtaining Pt nanoparticles with sodium borohydride. Guo et al. also prepared carbon-supported Pt nanocatalysts with sodium borohydride reduction method by employing citric acid as a stabilizer in ammonium hydroxide solution. It was reported that citric acid has an important role as a stabilizer and different concentrations of citric acid strongly influence the growth process of nanoparticles and their dispersion on carbon support and correspondingly the electrochemical performance of these catalytst. Besides these results, it was found that the annealing of these catalysts at 400 °C in an $N_2$ atm yields higher catalytic activity towards methanol oxidation reactions [12]. In another study, Jiang et al. prepared Pt nanocatalyst by using sodium citrate as stabilizer, with two different reducing agent, sodium borohydride and formaldehyde. It was found that Pt nanoparticles reduced by formaldehyde are smaller in size and more uniform in

dispersion compared to that reduced by sodium borohydride. This study also revealed that the citrate addition and its concentration influences the size and dispersion of Pt nanoparticles and consequently their catalytic activity as reported in literature before [24]. Deivaraj et al. prepared carbon-supported PtNi nanoparticles by employing hydrazine as a reducing agent under different conditions which are conventional heating, room temperature reduction, microwave-assisted reduction with the use of PVP as a stabilizer. According to this study, microwave reduction method yielded smaller and more uniform PtNi nanoparticles, and thereby the highest performance catalyst towards methanol oxidation reactions while hydrazine reduction method with conventional heating produced the poorest PtNi catalyst [30].

In our laboratory, carbon-supported Pt nanoparticles were prepared by superhydride reduction method to be employed as catalyst for a variety of alcohol oxidation reactions. These catalysts were obtained by changing some parameters such as metal precursor, surfactant or by inserting second metal such as Ru or Pd as promoter or by applying heat treatment after preparation. In order to investigate the influence of changing paramaters and conditions, it is essential to mention about the details of these studies. In a study, hexanethiol-stabilized Pt nanoparticles were synthesized by using two different metal precursors, $PtCl_4$ and $H_2PtCl_4$ and then heated to 200 °C, 300 °C and 400 °C to observe the effect of heat treatment on catalytic activity. It was found that precursor type does not change the particle size and catalytic activity, but heat treatment leads to an increase in particle size and a decrease in catalytic activity [31]. In another study, Pt nanoparticles were prepared by using $PtCl_4$ and $H_2PtCl_4$ as starting materials and heptanethiol, 1,1-dimethyl heptanethiol, hexadecanethiol and octadecanethiol as surfactants for methanol and ethanol oxidation reactions. It was found that the kind of surfactant directly affects the size of Pt nanoparticles and their catalytic activity. For instance, a branched surfactant, 1,1-dimethylheptanethiol, leads to an increase in particle size and catalytic activity as compared to linear surfactants owing to easy removal of branched surfactants from catalyst surface [32]. More recently, different kind of surfactants, hexylamine, heptylamine, decylamine, dodecylamine and their branched counterparts, were utilized for preparation of

carbon-supported Pt nanoparticles with the same methodology. It was found that the electrochemical performance of these catalysts is also dependent on the chain length and the branching degree of surfactants. It was reported that catalytic activity increases depending on the increase in degree of branching and decreases with increasing chain length, in other words, the catalyst stabilized by tertiary amine with a short chain demonstrates larger particle size and enhanced catalytic activity compared to that stabilized with linear and long chain amine surfactants as stated in previous works. However, the electrochemical performance of amine-stabilized catalysts was found to be higher than previously prepared thiol-stabilized ones due to different binding affinities of surfactants [33,34]. This data also supported by Yang et al. as reported above [27].

## 1.8. THE AIM OF PROJECT

The direct methanol fuel cell is often regarded as the ideal fuel cell system since it operates with the liquid fuel without bulky reformer system. However, the usage of DMFCs in commercial applications was hindered by the poor kinetics of anode reaction. This limitation in anode reaction directs the research focus on the investigation of active catalyst material for methanol oxidation reaction. It comes out that only Pt-based materials improve the poor kinetics of methanol oxidation [9]. For this purpose, in this thesis, a new type of carbon-supported Pt nanoparticles catalysts were prepared by using $PtCl_4$ as a starting material, sodium borohydride, hydrazine and formaldehyde as reducing agents and hexylamine, N-methylhexylamine, N,N-dimethylhexylamine as surfactants for methanol oxidation reaction. These catalysts were characterized by using a variety of techniques such as X-ray diffraction, transmission electron microscopy, X-ray photoelectron spectroscopy, cyclic voltammetry, chronoamperometry, BET surface area analysis, ICP, FTIR.

# CHAPTER 2

# EXPERIMENTAL

## 2.1. CHEMICALS

$PtCl_4$ (99 %, Alfa), $NaBH_4$ (96%, Merck), $N_2H_5OH$ (100%, Merck), formaldehyde (37%, Merck), NaOH (99%, Merck), toluene (99%, Merck), $C_2H_5OH$ (99.2%, Merck), $CH_3OH$ (99.8%, Merck), $CCl_4$ (99%, Merck), $HClO_4$ (60%, Merck), N,N-dimethylformamide (99.8%, Merck), hexylamine (99%, Sigma-Aldrich), N-methylhexylamine (96%, Sigma-Aldrich), N,N-dimethylhexylamine (98%, Sigma-Aldrich), nafion (5%, Sigma-Aldrich), VulcanCarbon (XC-72, Cabot Europa Ltd.) were used without any purification. Deionized water (18 MΩ) was obtained by Millipore water purification system.

## 2.2. PREPARATION OF CATALYSTS

### 2.2.1. PREPARATION OF CATALYST Ia

0.24 mmol (0.0808 g) of $PtCl_4$ as a starting material was dissolved in 120 mL of deionized water for 30 min under inert atmopshere. Then, 0.264 mmol of freshly prepared $NaBH_4$ solution (10% in excess ) with a concentration of 0.112 M was added to the solution dropwise to reduce Pt(IV) into Pt(0). The reduction was observed by change of color from light yellow to grayish black. Subsequently, 0.24 mmol hexylamine dissolved in 120 mL of toluene was added to the grayish black mixture. After addition of toluene, two immiscible layers were observed in the mixture and Pt nanoparticles were gathered between these two layers. In order to

observe more explicit phase seperation, 1.5 mL of 1 M NaOH solution was added to the mixture. After stirring for two hours, Pt nanoparticles were seperated by separation funnel and washed with dry ethanol (~50 mL) to remove the excess amine surfactants around nanoparticles. In washing process, Pt nanoparticles were sonicated in 50 mL of ethanol for 10 min and then centrifuged for 15 min to precipitate Pt nanoparticles in cloudy solution. This washing cycle was repeated six times by renewing ethanol until clear solution was obtained. Finally, precipitate involving Pt nanoparticles was dried under vacuum to remove ethanol.

### 2.2.2. PREPARATION OF CATALYST IIa

0.24 mmol of $PtCl_4$ precursor was dissolved in 120 mL of deionized water under argon atmosphere. Then, 2.4 mmol of 2 M $N_2H_5OH$ solution was added dropwise to the solution. The color turning from yellow to grayish black with each drop indicated formation of reduced Pt nanoparticles. Afterwards, 120 mL of toluene containing 0.24 mmol hexylamine was introduced into the solution. Then, the procedure was followed as in $NaBH_4$ case.

### 2.2.3. PREPARATION OF CATALYST IIIa

0.24 mmol $PtCl_4$ complex was dissolved in 120 mL of deionized water as in the other procedures. Then, the solution was heated up a temperature for optimum reduction, which was observed in vicinity of 68 °C. After the temperature was held around 68°C, the pH of solution was adjusted to 9-10 by adding 2.5 M NaOH solution to fulfill the required conditions for reduction. Then, 0.48 mmol of 13.43 M formaldehyde was added to the solution and stirred vigorously to initiate reduction. The reduction was monitored by color change as in the other cases. Afterwards, 120 mL of toluene containing 0.24 mmol hexylamine was added to the solution. The procedure was maintained by the same steps as mentioned above.

### 2.2.4. PREPARATION OF CATALYST Ib, Ic, IIb, IIc, IIIb, IIIc

The Catalysts Ib and Ic were prepared by reducing $PtCl_4$ with $NaBH_4$ as in section 2.2.1. N-methylhexylamine and N,N-dimethylhexylamine were used as surfactants for catalyst Ib and Ic, respectively. For Catalysts IIb and IIc, $N_2H_5OH$ was used as reducing agent and N-methylhexylamine, N,N-dimethylhexylamine as surfactants, respectively, as given in section 2.2.2.. Catalysts IIIb and IIIc were prepared by HCOOH (reducing agent) with the N-methylhexylamine, N,N-dimethylhexylamine as surfactants, respectively, as given in section 2.2.3. The name of catalysts, reducing agents and surfactants are given in Table 2.1.

**Table 2.1.** The name of catalysts, reducing agents and surfactants.

| Catalysts | Reducing agents | Surfactants |
|---|---|---|
| Catalyst Ia | $NaBH_4$ | Hexylamine |
| Catalyst Ib | | N-methylhexylamine |
| Catalyst Ic | | N,N-dimethylhexylamine |
| Catalyst IIa | Hydrazine | Hexylamine |
| Catalyst IIb | | N-methylhexylamine |
| Catalyst IIc | | N,N-dimethylhexylamine |
| Catalyst IIIa | Formaldehyde | Hexylamine |
| Catalyst IIIb | | N-methylhexylamine |
| Catalyst IIIc | | N,N-dimethylhexylamine |

### 2.3.PREPARATION OF ELECTRODE SOLUTION

36.78 mg of Pt-Carbon (with a ratio of 1:9) was mixed with 0.5 mL of nafion, 0.15 mL of N,N-dimethyl formamide and 2.5 mL of water. This mixture was sonicated in ultrasonic bath to obtain a highly dispersed colloidal solution. Then, 50μL of this slurry solution was dropped on the surface of glassy carbon electrode with 7 mm-

diameter and dried at 40 °C for 20 min, 65 °C for 20 min and 100 °C for an hour [35].

## 2.4. DETERMINATION OF PLATINUM CONTENT IN THE CATALYSTS

In order to determine the percentage of platinum in each catalysts, Leeman Lab inductively coupled plasma spectroscopy was used. The measurements were performed at METU Central Lab.

## 2.5. CHARACTERIZATION OF CATALYSTS

### 2.5.1. CYCLIC VOLTAMMETRY (CV)

Cyclic voltammetry is a common method to measure oxidation and reduction potentials of electroactive species. The fundamental principle of CV is based on measuring the current at working electrode by varying the potential exerted on it [36]. In CV measurements, a triangular potential waveform is exerted on working electrode as shown in Figure 2.1.

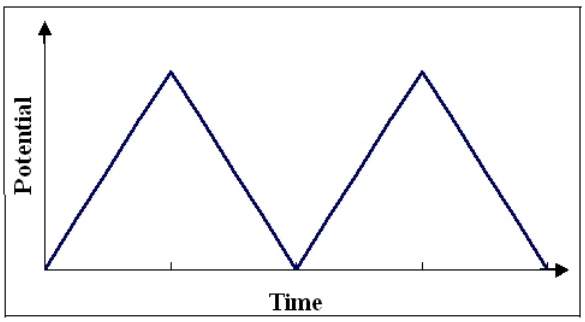


**Figure 2.1.** Triangular potential waveform [37].

The potential scan of working electrode with respect to reference electrode begins from a particular voltage value where any electrode reaction does not occur and moves to a voltage value at which oxidation or reduction occurs [38]. Then, the voltage goes linearly back to the starting value at the same rate. As a result of this

voltage variation in both forward and reverse directions, the surface of working electrode becomes sufficiently negative or positive with respect to reference and leads to electron transfer between solution species and electrode surface. This electron tranfer generates a measurable current in the circuit. As the voltage scan is reversed, direction of electron transfer is also reversed and inverse peak current is obtained [36]. A typical cylic voltammogram with oxidation-reduction peaks is shown in Figure 2.2.

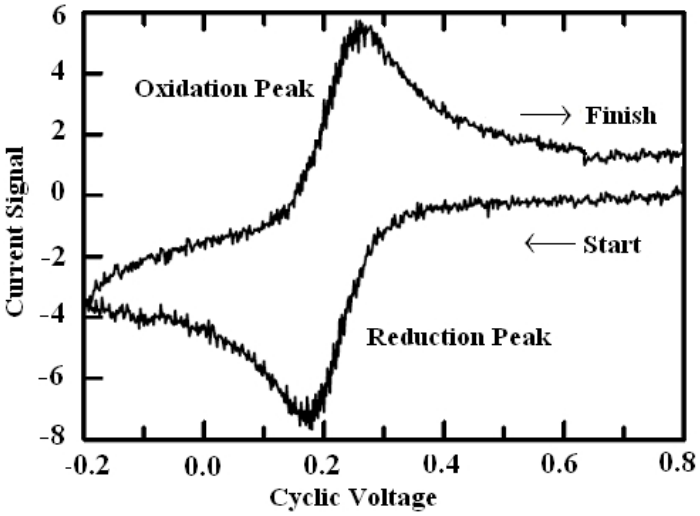


**Figure 2.2.** A cyclic voltammogram with oxidation and reduction peaks [10].

### 2.5.1.1. ELECTROCHEMICAL CELL

In CV measurements, a three-electrode system consisting of working electrode, reference electrode and counter electrode was used. Prepared catalysts dispersed on 7 mm of glassy carbon were used as working electrodes. Saturated calomel electrode (SCE) and glassy carbon were used as reference and counter electrodes, respectively. Measurements were carried out in both 0.1 M $HClO_4$ and 0.1 M $HClO_4$ + 0.5 M $CH_3OH$ electrolyte solutions for each catalyst at room temperature using computer-controlled potentiostat/galvanostat (Solartron 1285) in Chemistry Department of METU. Before each measurement, electrochemical cell system was purged with pure argon gas for 10 min to remove oxygen.

### 2.5.2. CHRONOAMPEROMETRY (CA)

Chronoamperometry is used to examine the stability of initital redox states of compounds in a potential range. The measurement is done by recording the switching on current versus time. By this technique, the potential range in which no faradaic and only capacitance current are observed is distinguished from the higher faradaic currents detected due to oxidation or reduction reactions [39]. For CA measurements, the excitation voltage signal in the form of square wave is applied to working electrode and the corrresponding current decay is recorded upon the potential applied [36,40].

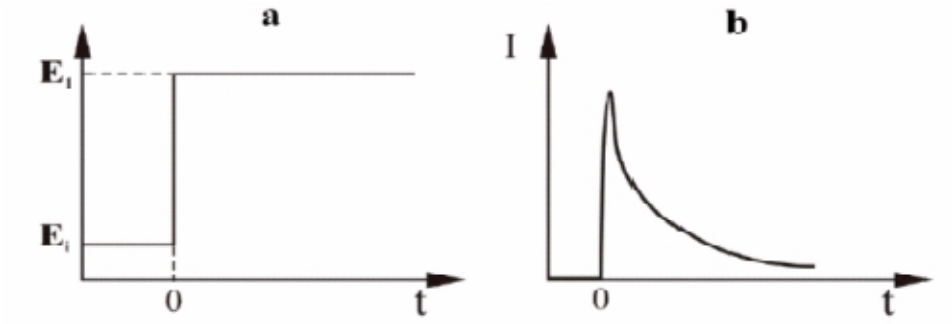


**Figure 2.3.** a) Excitation voltage signal in square wave form vs time b) a typical chronoamperogram [40].

In this study, CA measurements were done with three-electrode system in 0.1 M $HClO_4$ + 0.5 M $CH_3OH$ electrolyte solution as described in section 2.5.2.1.

### 2.5.3. X-RAY DIFFRACTION (XRD)

XRD is a powerful and nondestructive tool used for fingerprint identification of crystalline materials and determination of their structure [41]. Each crystalline material has unique XRD pattern which allows the determination of lattice parameters, orientation, crystallite size and the other structrual parameters [42]. In XRD technique, the sample is illuminated by X-ray in a fixed wavelength and then

the radiation scattered back. When the scattered radiation undergoes constructive interference, diffraction peaks occurs at certain angles satisfying Bragg's law:

$n\lambda = 2d\sin\theta$

where, n is an integer, λ is the wavelength of the X-ray, d is the spacing of crystal layers and θ is the incident angle [43, 44].

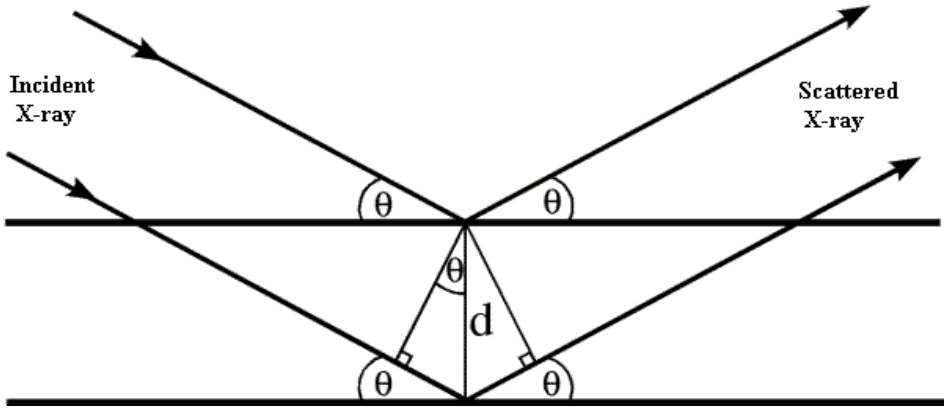


**Figure 2.4.** Incident and scattered X-rays [24].

In this study, the average particle size of Pt catalysts were calculated by using Scherrer equation:

$d = k\lambda / \beta\cos\theta$

where d is average particle size, k is a constant (0.9), λ is the wavelength of incident X-ray, β is half width of XRD peak in radian and θ is the angle of peak at maximum height. XRD measurements were carried out by using Rigaku Miniflex diffractometer with Ultima + theta-theta high resolution goniometer and X-ray source (Cu Kα radiation, λ= 1.54056 Å) in chemistry department at METU [45].

### 2.5.4. TRANSMISSION ELECTRON MICROSCOPY (TEM)

Transmission electron microscope is an indispensable instrument for imaging of nanostructured materials at atomic level to obtain structural and chemical information [46]. The basic principle of TEM is analogue to light-optical microscope but electron source is used intead of light source. Furthermore, electromagnetic lenses take the place of glass lenses used in light microscope [47].

In transmission electron microscopy, a beam of electron is accelerated to high energy level at high voltage and focused on a thin specimen within a high vacuum. The transmitted electrons through the specimen hit on a flourescent screen as a magnified image of specimen. These magnified images with atomic level resolution provide information about crystal structure and orientation of specimen and chemical composition of phases [47-49].

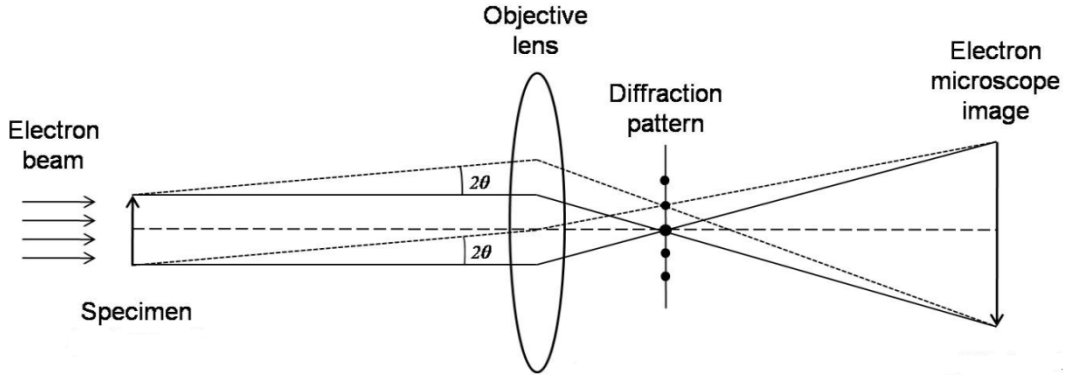


**Figure 2.5.** Schematic representation of transmission electron microscope [50].

In this study, carbon supported Pt catalysts were sonicated in $CCl_4$ for 6 hours until particles in solvent has reached a finely divided form. Then, this mixture was dropped on copper grid with 400 mesh and dried at room temperature. TEM images of these samples were taken by JEOL 200 kV TEM instrument in Central Lab. at METU.

### 2.5.5. X-RAY PHOTOELECTRON SPECTROSCOPY (XPS)

X-ray photoelectron spectroscopy is powerful analytical technique to study the surface of materials by ejecting electrons from core level of surface by irradiating with X-ray radiation source. In this technique, energy of incident photon is sent to the solid sample surface and transferred to core electron. If the energy of photon is greater than the binding energy of electron, the electrons are ejected from core shell of surface since they have enough energy to leave sample. Due to emission of electron, core shell is ionized as follows:

$$A + h\nu \rightarrow A^{+} + e^{-}$$

The energy conservation requires:

$$E(A) + h\nu \rightarrow E(A^{+}) + E(e^{-})$$

$$E_K = h\nu - [E(A^{+}) + E(e^{-})] - \phi$$

$$E_k = h\nu - E_B - \phi$$

where $E_B$ is the binding energy relative to the fermi level and $E_K$ is the kinetic energy of the photoelectron relative to vacuum level. The photoelectron spectrum is given by the kinetic energy distribution of the photoelectrons ejected from core shells. This kinetic energy is characteristic for the element. In this manner, for a known photon energy (hν) the binding energy can be estimated for all core electrons. Energy analysis of the emitted electrons is the primary data used for XPS [51,52].

An XPS spectrum provides information about chemical composition of sample, oxidation state of elements in sample, the density of electronic states, binding energies of one or more electronic states for all elements except hydrogen and helium due to their small diameter of orbital [53].

### 2.5.6. BRANAUER-EMMETT-TELLER (BET) SURFACE AREA ANALYSIS

The BET method is a significant analysis tool for measurement of specific surface area of ultra-fine powders or mesoporous solid materials. The BET method was developed by Stephen Braunauer, Paul Emmett and Edward Teller. The theory of this method is essentially based on the Langmuir theory that explains the adsorption of gas molecules on a solid surface in monolayer at a given pressure. The BET theory extends the Langmuir theory to multilayer adsorption with the additional assumptions: (1) gas molecules physically adsorbed on a solid surface as infinite layers without interaction between different adsorption layers; (2) the Langmuir theory can be applied to each layer. The resulting BET isotherm gives the amount of gas adsorbed as a function of the relative pressure. The BET equation utilizes the data from the isotherm to determine the surface area of sample [54-56].

$$\frac{1}{V[(Po - P) - 1]} = \frac{C - 1}{VmC}\left(\frac{P}{Po}\right) + \frac{1}{VmC}$$

where P and Po are equilibrium and saturated pressure of gas adsorbed at adsorption temperature, V is the adsorbed gas amount in volume units, Vm is the monolayer adsorbed gas amount, C is dimensionless constant related to the enthalpy of adsorbtion of adsorbate gas on the powder sample.

In BET analysis, Nitrogen is the most common gas used for adsorption due to its availability in high purity and its strong interaction with solids. The other gaseous materials can also be used for adsorption in some circumstances. The BET analysis provides significant information for understanding of structure, formation and potential use of different materials [56,57]

### 2.5.7. FOURIER TRANSFORM INFRARED SPECTROSCOPY (FTIR)

FTIR spectroscopy is a useful technique for idenfiying the structure of materials. In this technique, infrared light is sent through a sample. As illustrated in Figure 2.6., some of the light is absorbed by the sample and the remaining light is transmitted. As a result, an infrared spectrum is obtained with absorption peaks representing the frequencies of vibrations between the bonds of atoms involved in the material. Each different material exhibits characteristic infrared spectrum. Therefore, this technique provides qualitative and quantitative information about the material by utilizing the size of peaks in the spectrum [53,58].

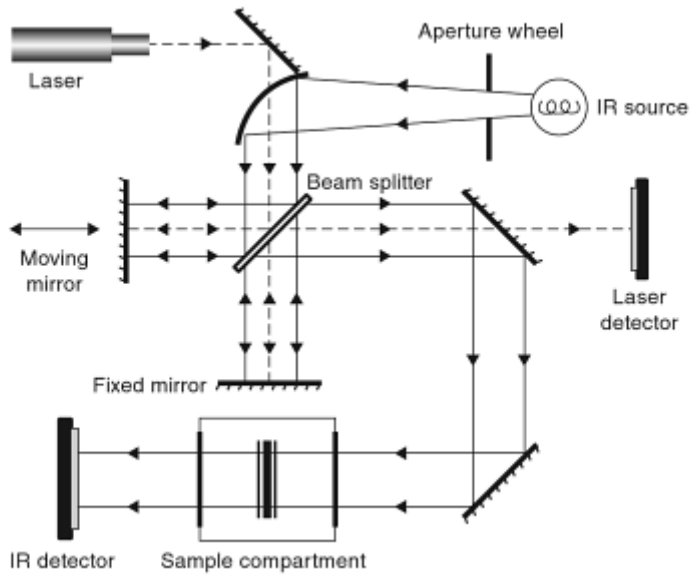


**Figure 2.6.** The principle of FTIR spectroscopy [59].

There are two types of infrared instruments. In dispersive-type spectrometer, a grating works as a prism and disperse visible light into its individual frequencies. The detector measures each frequency which passed through the sample. In fourier transform infrared spectrometer, all of the infrared frequencies are measured simultaneously, rather than indivudually by using interferometer. The corresponding signal is named as interferogram and interpreted via mathematical algorithm called Fourier transform. In this thesis, FTIR spectra were measured by Bruker 66 v/s by using KBr pellets with 15 scans at room temperature [10].

# CHAPTER 3

# RESULTS AND DISCUSSION

## 3.1. INDUCTIVELY COUPLED PLASMA SPECTROSCOPY AND BET SURFACE AREA ANALYSIS

In order to determine the platinum content of each catalyst, inductively coupled plasma spectroscopy was used and the results were given in Table 3.1. As it can be seen from the table, the catalysts nearly contain about 90% platinum. The remaining 10% contamination may come from unremoved chemicals such as surfactant. These platinum content results were used to define the current density of catalysts (A/mg Pt) for CV measurements.

Furthermore, the total surface area of each catalyst was determined by BET surface area analysis and given in Table 3.1. As shown in the table, the largest surface area was detected for Group I catalysts (30 - 35 $m^2/g$) while the smallest surface area was observed for Group II catalysts (4 - 10 $m^2/g$). For each group, the effect of surfactant on the surface area was also investigated and it has been found that there is no direct relationship between the kind of surfactants and surface area of catalysts. This shows that the dominant factor on the surface area of catalysts is the kind of reducing agent not surfactants.

**Table 3.1.** The platinum content and the total surface area of all prepared catalysts.

| Catalysts | Platin content (%) | Surface area ($m^2/g$) |
|---|---|---|
| Catalyst Ia | 93.8 ± 1.5 | 35.22 |
| Catalyst Ib | 88.3 ± 2.1 | 30.64 |
| Catalyst Ic | 89.4 ± 1.4 | 32.79 |
| Catalyst IIa | 91.8 ± 0.6 | 9.503 |
| Catalyst IIb | 90.8 ± 1.0 | 6.478 |
| Catalyst IIc | 92.5 ± 0.5 | 3.791 |
| Catalyst IIIa | 90.0 ± 0.6 | 21.00 |
| Catalyst IIIb | 88.5 ± 0.7 | 29.82 |
| Catalyst IIIc | 91.0 ± 0.4 | 19.35 |

## 3.2. FOURIER TRANSFORM INFRARED SPECTROSCOPY

In order to investigate the species around Pt nanoparticles, FTIR spectra of Catalyst Ia, Ib, Ic, IIa, IIb, IIc, IIIa, IIIb, IIIc, hexylamine, N-methylhexylamine and N,N-dimethylhexylamine were recorded and shown in Figures 3.1.a. As can be seen from the figure, it does not matter which reducing agents and surfactants are used, the FTIR spectra of all catalysts are very similar. In order to define the origin of the peaks, the spectra of Carbon XC-72 catalysts and Catalyst IIIb, which represents all the prepared catalysts were compared in Figure 3.1.b. and found that they have quite similar FTIR pattern. This shows that surfactants and other materials, which are found in chemical reaction medium, decompose and form partially crystalline carbon black during the chemical process (reaction).

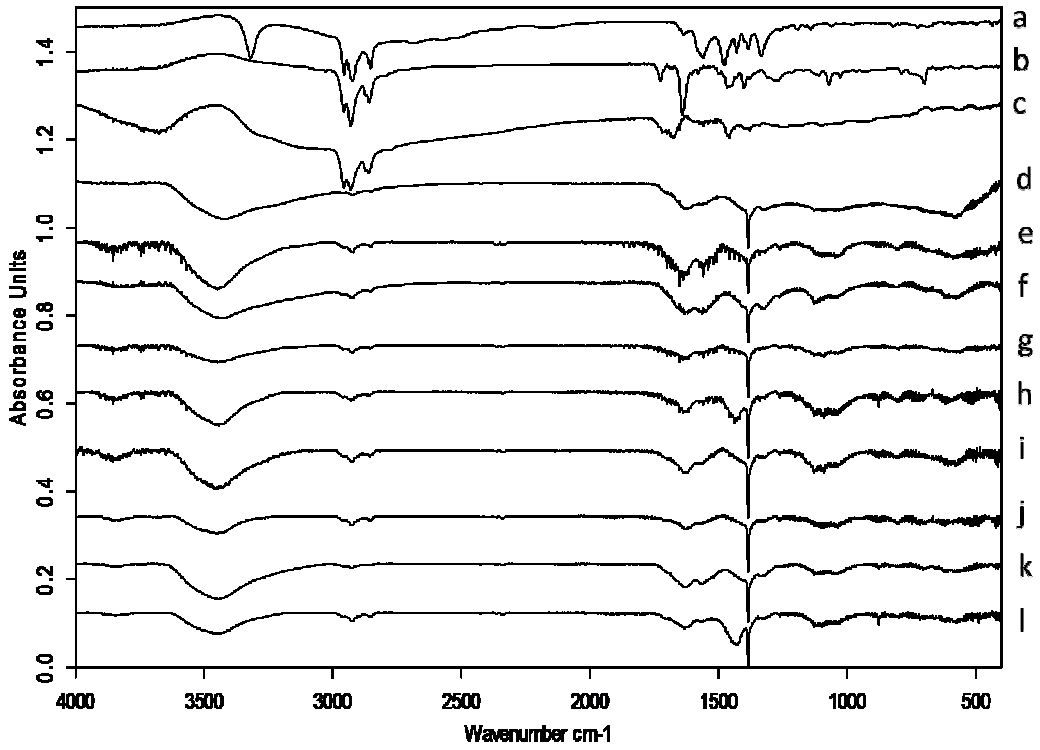


**Figure 3.1.a.** FTIR spectra of a) hexylamine, b) N-methylhexylamine c) N,N-dimethylhexylamine, d) Catalyst Ia, e) Catalyst Ib f) Catalyst Ic, g) Catalyst IIa, h) Catalyst IIb, i) Catalyst IIc, j) Catalyst IIIa, k) Catalyst IIIb, l) Catalyst IIIc.

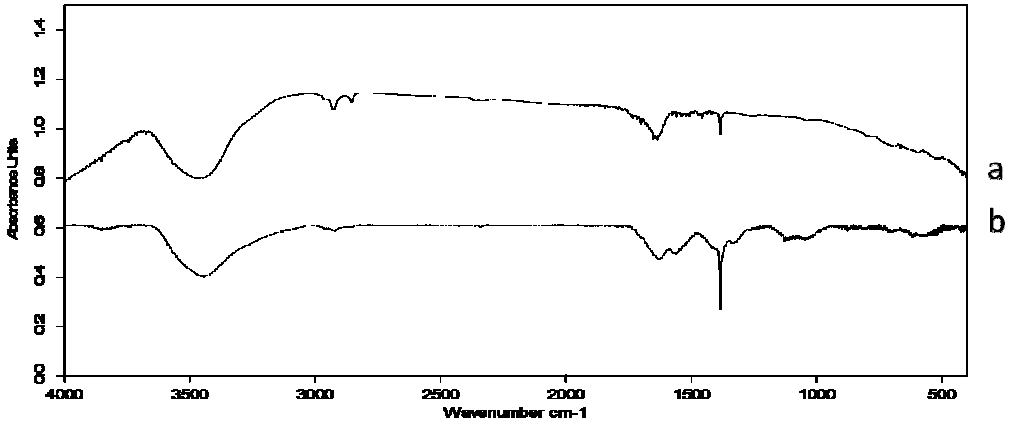


**Figure 3.1.b.** FTIR spectra of a) Carbon XC-72, b) Catalyst IIIb.

## 3.3. X-RAY DIFFRACTION AND TRANSMISSION ELECTRON MICROSCOPY

In order to determine crystal structure and average particle size of prepared catalysts, X-ray diffraction method was utilized. The powder XRD patterns of all catalysts exhibit typical crystalline peaks of face-centered cubic (fcc) Pt at about 2θ of 39.8, 46.3, 67.9, 81,5 which correspond to Pt(111), Pt(200), Pt(220) and Pt(311) planes of fcc Pt, respectively, as shown in Figure 3.1. [45]. The average particle size of Pt nanoparticles was calculated from full width half-maximum of Pt(220) diffraction peak of each catalyst by using Scherrer Formula [60];

$$d = \frac{k\lambda}{\beta \cos\theta}$$

where, d is average particle size, k is Scherrer constant (0.9), λ is wavelength of incident X-ray (1.54056 Å ), β is the full width half-maximum of XRD peak (rad) and θ is the angle of peak at maximum height.

The average particle size of Catalyst Ia, Ib, Ic, IIa, IIb, IIc, IIIa, IIIb and IIIc was determined as ~5.3, ~5.5, ~5.2, ~4.1, ~4.9, ~4.5, ~5.2, ~4.1 and ~4.9 nm, respectively, Table 3.2. As it can be seen from XRD results, the average platinum nanoparticle size of the catalysts was found to be quite close to each other, which ever reducing agent and surfactant were used. The average size of platinum nanoparticles is consistent with the literature data. For example, Yang et al. also prepared platinum nanoparticles using phase transfer method and used $NaBH_4$ as a reducing agent and found that the average particle size of platinum nanoparticles are in the range of 4 - 6 nm [61-63].

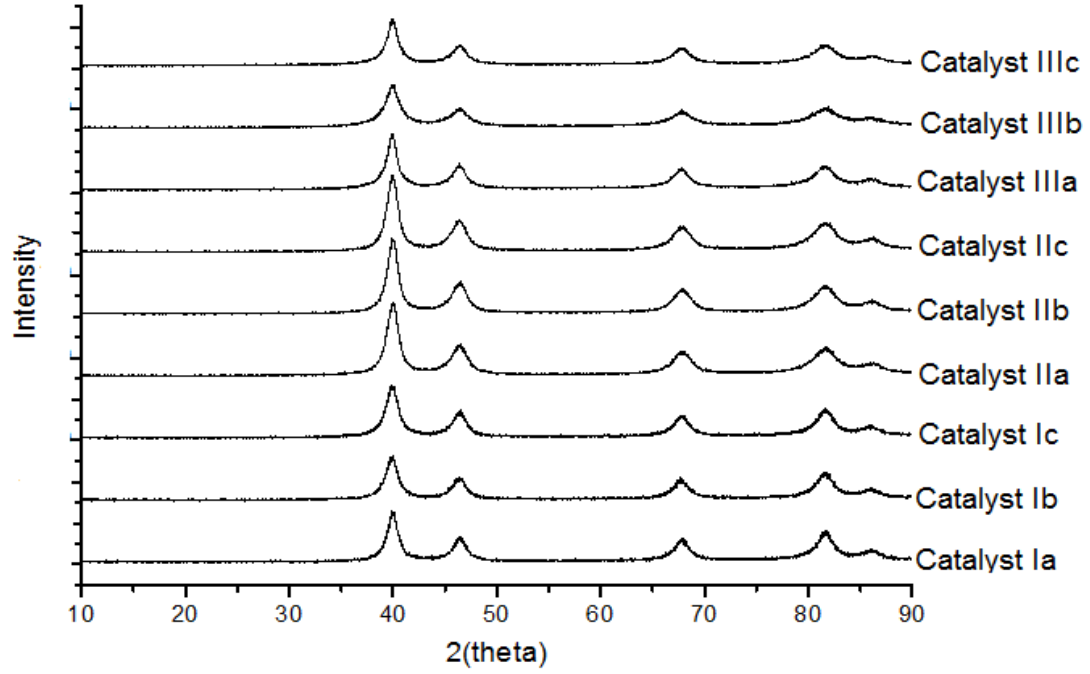


**Figure 3.2.** X-ray diffraction patterns of Catalyst Ia, Ib, Ic, IIa, IIb, IIc, IIIa, IIIb and IIIc.

In order to observe individual particle size of Pt nanoparticles and its distribution on carbon support, high resolution transmission electron microscopy was used. The representative TEM images and the particle size histograms obtained from the TEM images were given in Figure 3.2.a.b.c. The average particle size of small platinum nanoparticles in Catalysts Ia, Ib, Ic, IIa, IIb, IIc, IIIa, IIIb and IIIc was found to be ~4.9, 5.1, 4.9, 4.0, 4.6, 4.6, 4.8, 4.3 and 4.9 nm, respectively, Table 3.2. As can be seen from the table, there is not much difference between TEM and XRD results when only the small particles are considered. It should be stressed that it is not possible to determine exact size of platinum nanoparticles by XRD, if there is a broad range of particle sizes [31]. As emphasized above, however, it is possible to observe the individual particles by TEM. The transmission electron micrograph analysis revealed that the morphology of platinum nanoparticles depends on the reducing agent that is used during preparation method not surfactants. Three different kind of reducing agents were used, therefore, there are three different types of platinum nanoparticles' morphology exist in the prepared catalysts.

The first group contains Catalysts Ia, Ib and Ic which were prepared by using $NaBH_4$ as a reducing agent. The platinum nanoparticles in this group were mostly observed in cubic shape, Figure 3.3.a. and the same kind of particles were also observed by Yang et al. [61]. The size of cubic platinum nanoparticles was determined in a range altering from 3 nm to 7 nm. Besides these small cubic nanoparticles, it was also possible to observe an agglomeration of these small particles. The shape of agglomerated particles were no perfect spherical, therefore, it was not possible to draw a histogram for this group. However it is still possible to give the rough size of the agglomerated platinum nanoparticles, such as it is in the range of 20 nm - 200 nm. These agglomerated particles on carbon support were observed as sparsely dispersed clumps in random shapes.

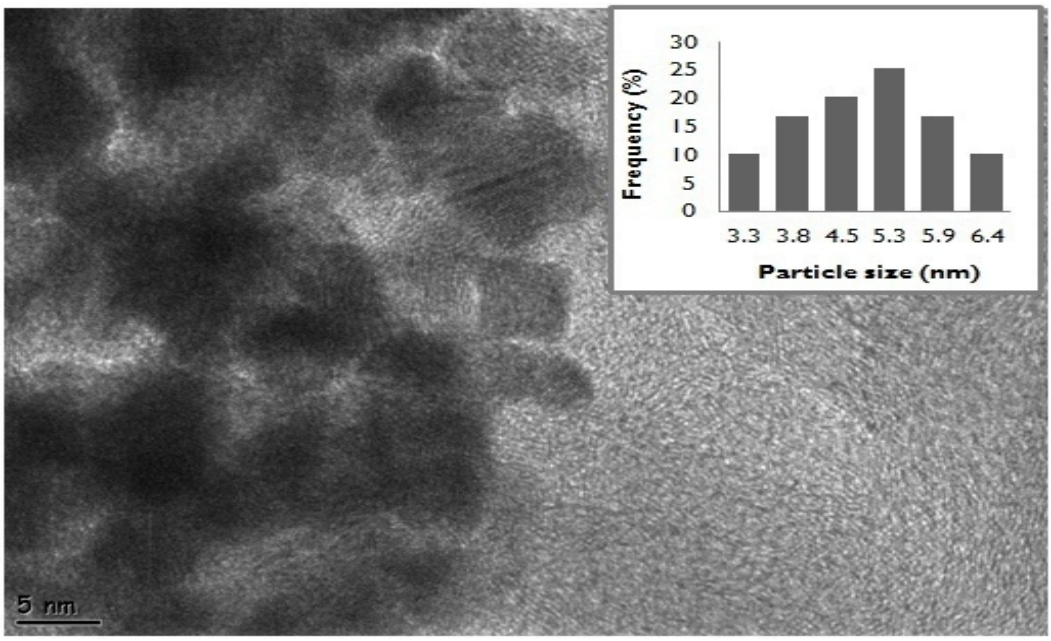


**Figure 3.3.a.** TEM image and particle size distribution histogram of Catalyst Ic.

The second group involves Catalyst IIa, IIb and IIc which were prepared by reduction of $PtCl_4$ by hydrazine. In this group, most of the Pt nanoparticles are large, dense (compact) and spherical agglomerated pieces with a size of 50 nm to 200 nm. The size distribution of these agglomerated Pt nanoparticles are given in histogram, Figure 3.4. In addition to these compact large lumps, it is also possible to observe less intense agglomerated platinum particles which is formed by stacking of many

individual platinum nanoparticles with a size of 2 - 5 nm. Besides these compact and less dense large particles, there are small amount of tiny Pt nanoparticles, ~4 nm. This type of morphology clearly indicates that the active surface area of this group of catalyst is small which is supported by BET analysis, 4 - 10 $m^2/g$.

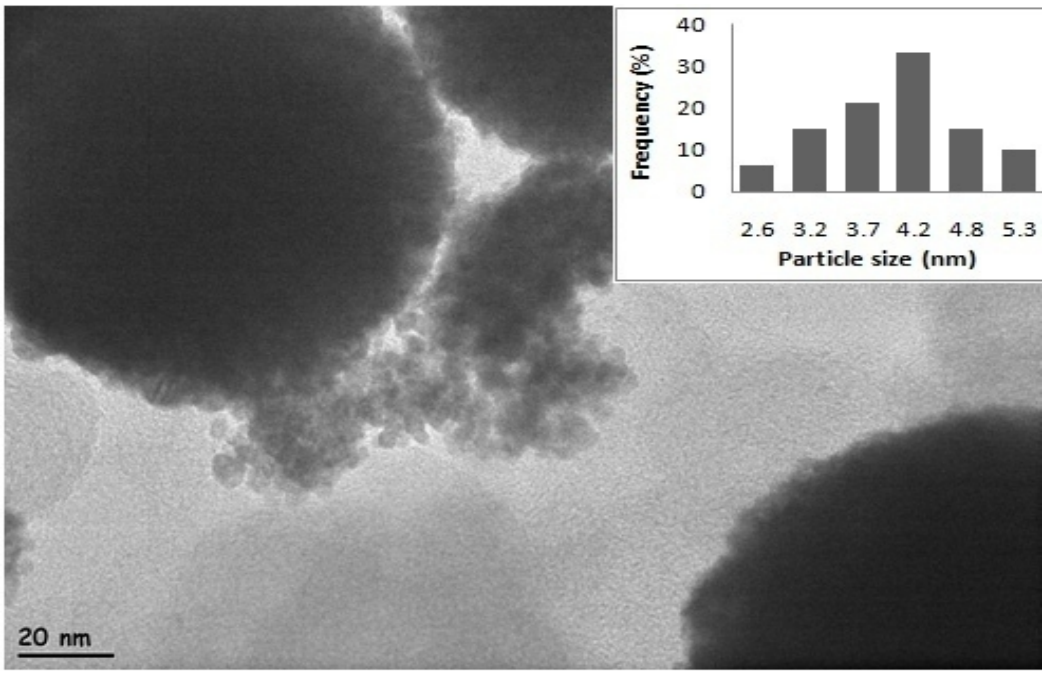


**Figure 3.3.b.** TEM image and particle size distribution histogram of Catalyst IIa.

The last group contains Catalysts IIIa, IIIb and IIIc in which formaldehyde were used as a reducing agent. TEM images of this group catalysts indicated that there are considerable number of small spherical nanoparticles dispersed on carbon support uniformly. The size of these well-dispersed particles was observed between 3 nm and 5 nm from size distribution histogram in Figure 3.3.c. In addition, the agglomerated particles mostly in spherical shape were observed in a size range of 50 nm - 150 nm on some part of carbon support. The size distribution histograms of these agglomerated particles were given in Figure 3.4. However, these large particles were not intense and frequent as in Catalysts IIa, IIb and IIc. As expected, BET analysis showed that the active surface area of Group III catalysts (20 - 30 $m^2/g$) is larger than Group II catalysts (4 - 10 $m^2/g$).

Moreover, the crystallinity of Pt nanoparticles was confirmed by measuring lattice fringe spacing of (111) and (200) planes. As shown in Figure 3.3.c., the lattice fringe spacing of (111) and (200) planes was measured as 0.219 nm and 0.196 nm for Catalyst IIIb, respectively. These values are consistent with nominal d-spacing values of Pt (111) and Pt (200) planes of fcc Pt, which are 0.227 nm and 0.197 nm, respectively [64,65].

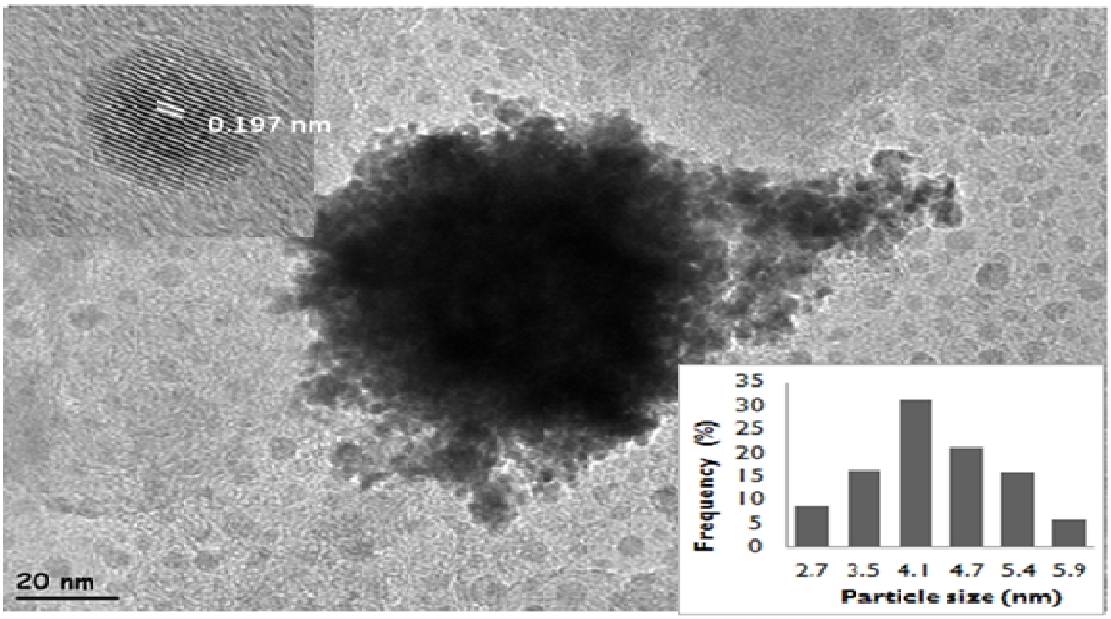


**Figure 3.3.c.** TEM image and particle size distribution histogram of Catalyst IIIb.

**Table 3.2.** Average particle size of platinum nanoparticles estimated by a) XRD and b) TEM ( Agglomerated particles are not considered)

| Catalysts | a | b |
|---|---|---|
| Catalyst Ia | ~ 5.3 nm | ~ 4.9 ± 1.0 nm |
| Catalyst Ib | ~ 5.5 nm | ~ 5.1 ± 0.8 nm |
| Catalyst Ic | ~ 5.2 nm | ~ 4.9 ± 0.9 nm |
| Catalyst IIa | ~ 4.1 nm | ~ 4.0 ± 0.7 nm |
| Catalyst IIb | ~ 4.9 nm | ~ 4.6 ± 0.6 nm |
| Catalyst IIc | ~ 4.5 nm | ~ 4.6 ± 0.8 nm |
| Catalyst IIIa | ~ 5.2 nm | ~ 4.8 ± 0.7 nm |
| Catalyst IIIb | ~ 4.1 nm | ~ 4.3 ± 0.8 nm |
| Catalyst IIIc | ~ 4.9 nm | ~ 4.9 ± 0.7 nm |

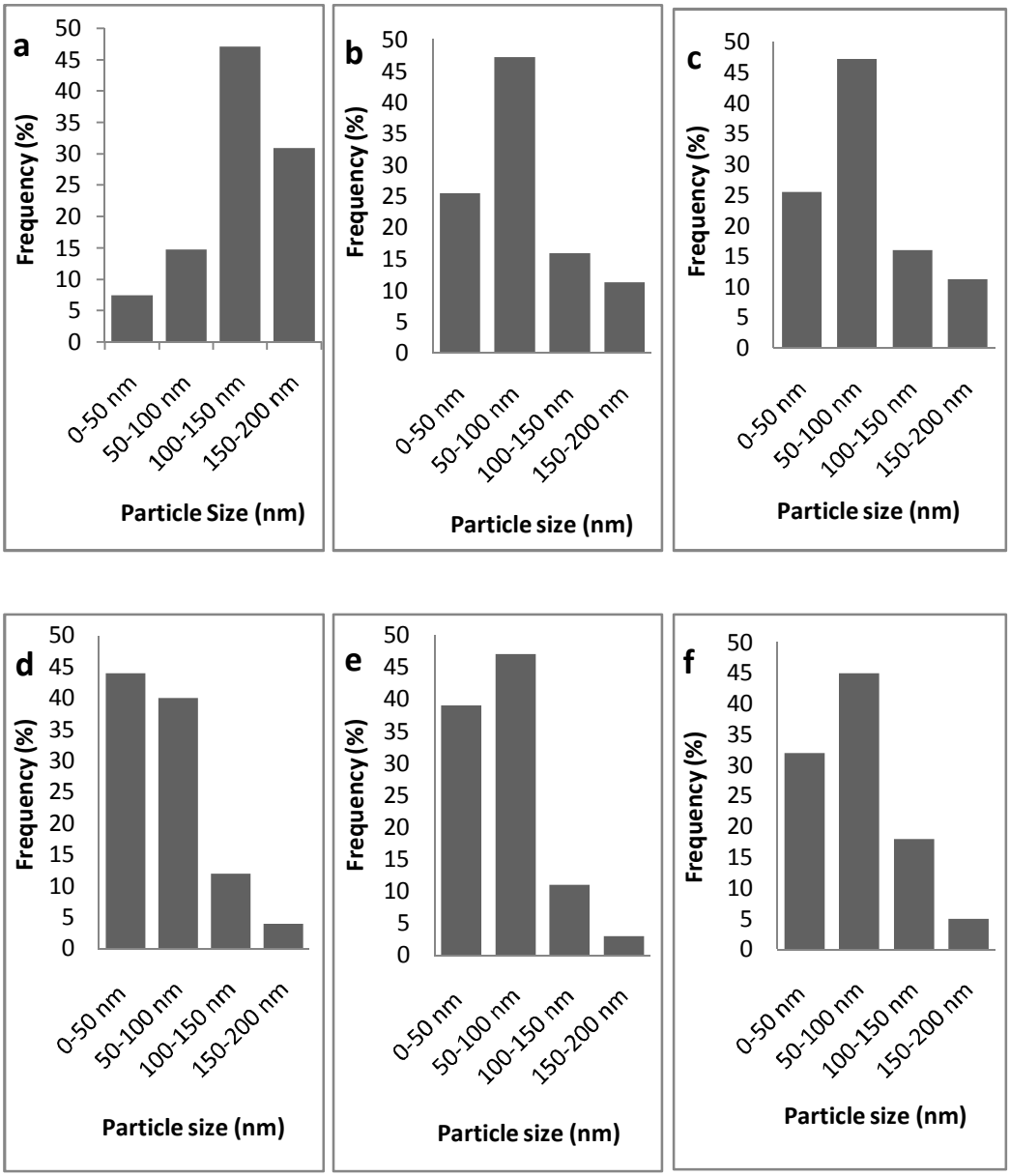


**Figure 3.4.** The size distrubution histograms of agglomerated particles in a) Catalyst IIa, b) Catalysts IIb, c) Catalyst IIc, d) Catalyst IIIa, e) Catalyst IIIb and f) Catalyst IIIc.

### 3.4. X-RAY PHOTOELECTRON SPECTROSCOPY

In order to examine the elemental composition and environment of surface of the catalysts, X-ray photoelectron spectroscopy was utilized. In all cases, XPS survey spectra of catalysts were recorded in broad range of energy and revealed platinum, oxygen and carbon signals, Figure 3.5. The high resolution XPS spectra of Pt 4f, O 1s, C 1s regions were also recorded. The existence of carbon peak with the C 1s binding energy of 284.5 eV showed the presence of carbon in all catalysts due to unremoved surfactant residues around the surface of catalysts despite extensive washing. The Pt 4f and O 1s regions of XPS spectra were further analyzed to acquire detailed information about the composition of catalysts.

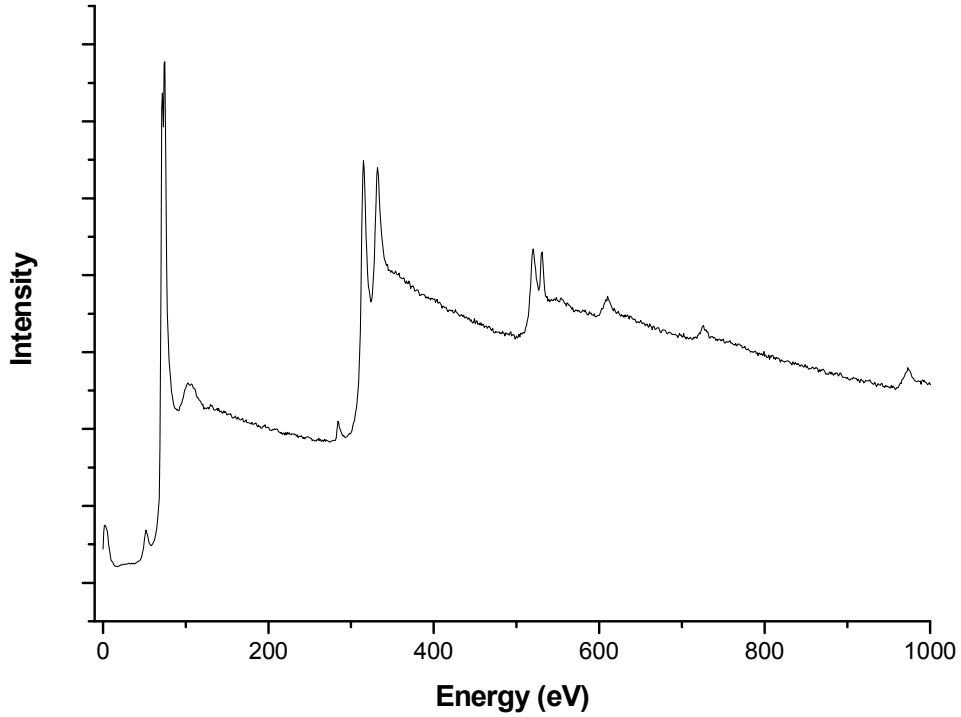


**Figure 3.5.** Broad range X-ray photoelectron spectra of Catalyst Ia.

In order to determine oxidation states of platinum nanoparticles in the catalysts and their relative intensities, Pt 4f region of XPS scan was fitted by Gaussian-Lorentzian method due to asymmetric line shapes of peaks in spectrum. As a result of curve fitting analysis, the spectrum could be resolved into two pairs of doublet with an energy seperation of 3.35 eV and the relative peak intensity of ca. 3:4 due to the presence of different oxidation states in catalysts as illustrated in Figures 3.6.a.b.c. The more intense doublet peaks with binding energies of 71.1eV ($4f_{7/2}$) and 74.4 eV ($4f_{5/2}$) are attributed to zero-valent state of Pt while the second doublet peaks around 74.5eV ($4f_{7/2}$) and 77.6eV ($4f_{5/2}$) are assigned to Pt(IV) species such as $PtO_2$ and/or $Pt(OH)_4$. Previous studies revealed that Pt $4f_{7/2}$ peak at 74.4 eV is associated with $Pt(OH)_4$ and Pt $4f_{7/2}$ peak between 74.6 - 74.9 eV is ascribed to $PtO_2$ on the catalyst surface [25,32,66]. The binding energies of Pt(0) and Pt(IV) species in the catalysts are shown in Table 3.3. As can be seen from table, there is no significant shift at peak positions of Pt(0) and Pt(IV) peaks [33]. The ratios of Pt(0) to Pt(IV) was determined by integrating relative areas of doublet peaks and given in Table 3.3. This ratio was found to be in the range of 65.1-71.3:34.9-28.7 for all prepared catalysts. These results indicated that metallic Pt(0) is the predominant species in all the catalysts.

**Table 3.3.** Pt $4f_{7/2}$ core binding energies, eV, in all prepared catalysts and the relative intensities of species on catalyst surface.

| | Pt $4f_{7/2}$ | Pt $4f_{7/2}$ |
|---|---|---|
| Catalysts | Pt (0) | Pt(IV) |
| Catalyst Ia | 71.2 (65.1) | 74.5 (34.9) |
| Catalyst Ib | 71.1 (65.5) | 74.4 (34.5) |
| Catalyst Ic | 71.1 (65.1) | 74.4 (34.9) |
| Catalyst IIa | 71.1 (68.9) | 74.4 (31.1) |
| Catalyst IIb | 71.2 (71.3) | 74.5 (28.7) |
| Catalyst IIc | 71.0 (69.6) | 74.4 (30.4) |
| Catalyst IIIa | 71.0 (65.6) | 74.3 (34.4) |
| Catalyst IIIb | 71.2 (69.1) | 74.5 (30.9) |
| Catalyst IIIc | 71.2 (69) | 74.5 (31) |

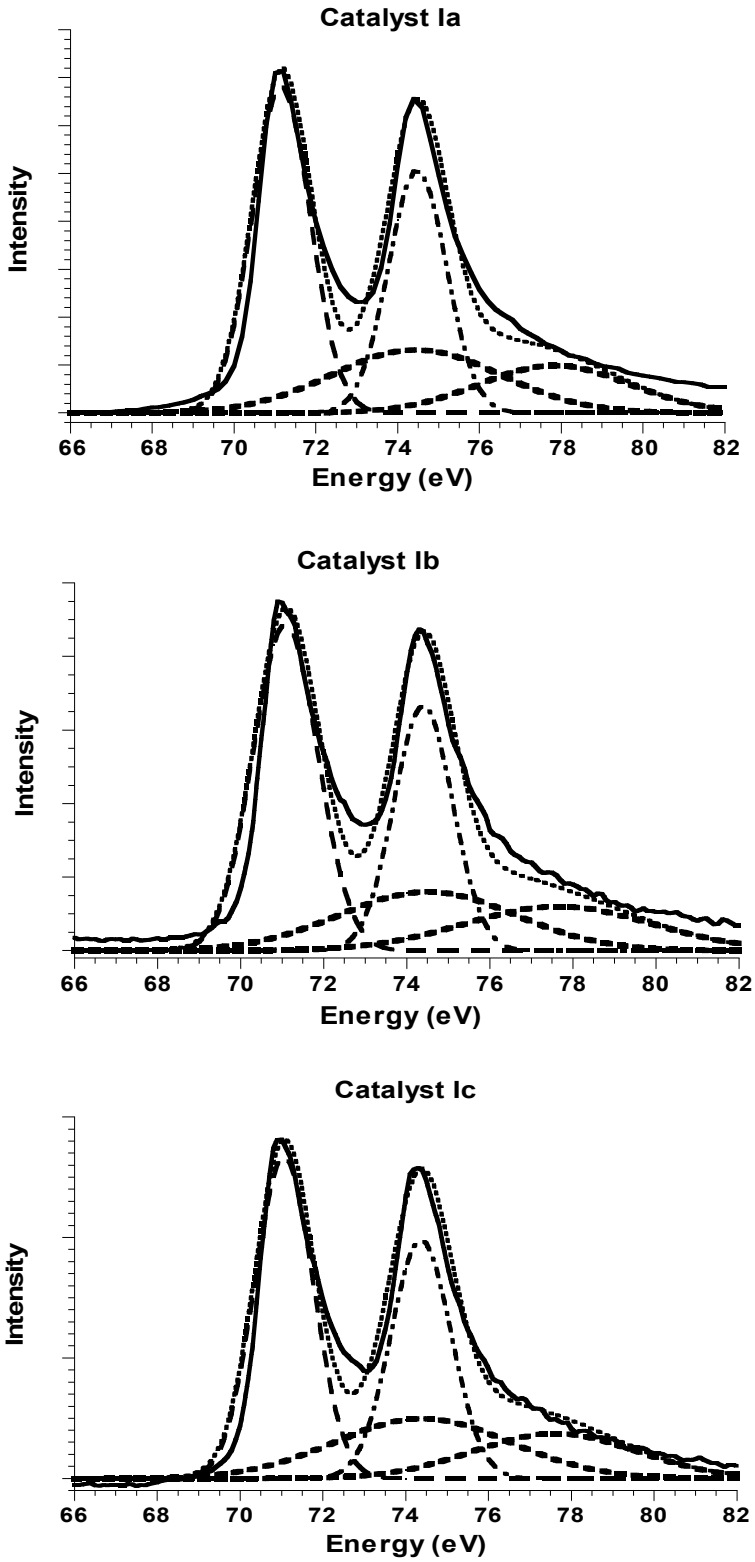


**Figure 3.6.a.** Pt 4f electron spectra of Catalyst Ia, Ib and Ic.

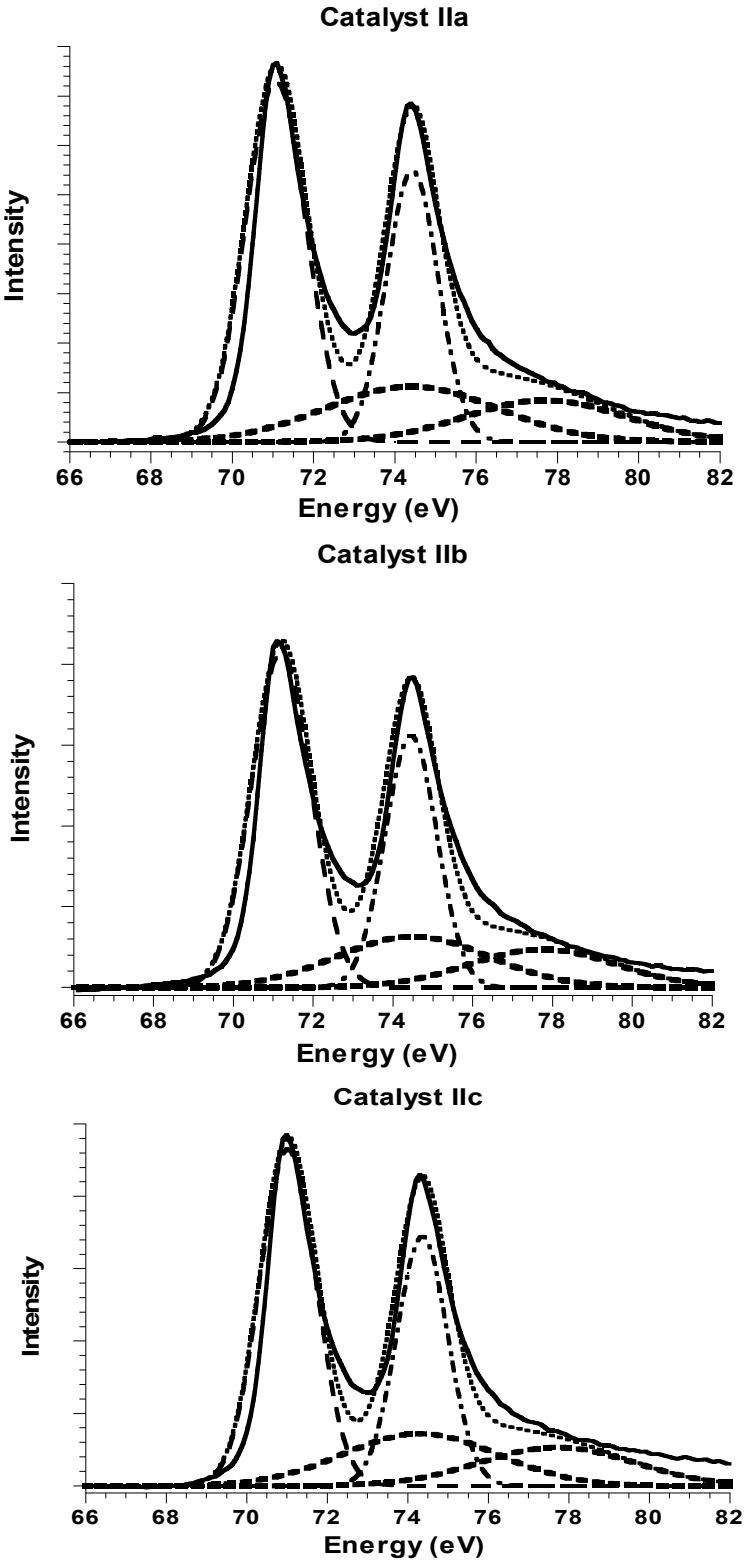


**Figure 3.6.b.** Pt 4f electron spectra of Catalysts IIa, IIb and IIc.

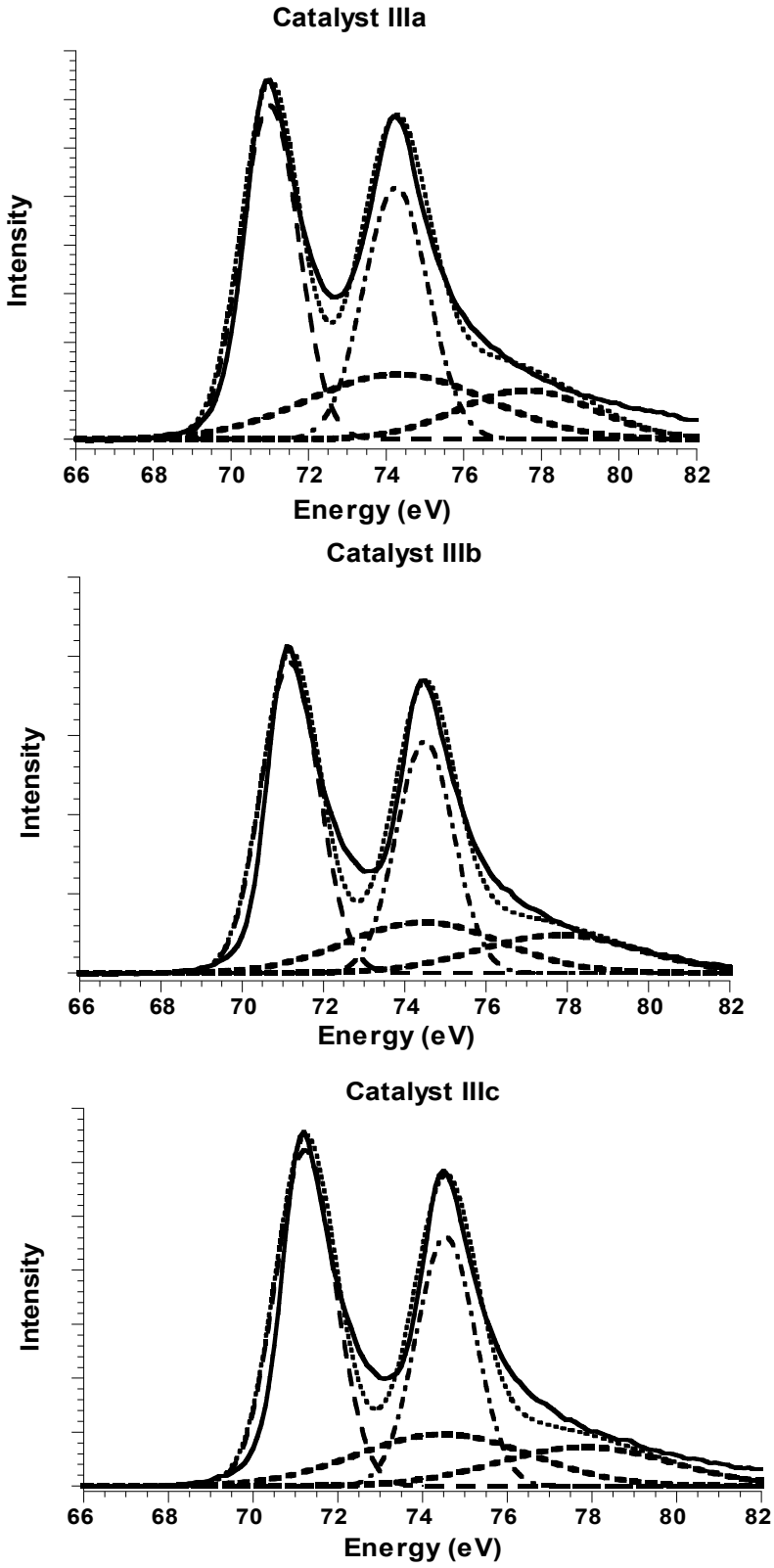


**Figure 3.6.c.** Pt 4f electron spectra of Catalysts IIIa, IIIb and IIIc.

The O 1s regions of XPS spectra were analyzed for all prepared catalysts. The O 1s region could be resolved into two peaks with an energy seperation of about 1.6 eV by the help of Gaussian curve fitting analysis, Figures 3.7.a.b.c. The binding energies and the relative integrated intensities of peaks are given in Table 3.4. As it can be seen from the table, the first peaks were observed between 531.1 - 531.5 eV and the second peaks were seen at about 533.2 eV. Previous studies revealed that the peaks with the binding energy at about 531.5 ± 0.5 eV are attributed to adsorbed hydroxide ($HO_{ads}$) on platinum surface and the peaks at about 533.0 ± 1.0 eV are assigned to adsorbed water ($H_2O_{ads}$) [67,68]. The amount of $HO_{ads}$ and $H_2O_{ads}$ on the surface of the catalysts were calculated by using the area under each peak and it was found that the amount of $H_2O_{ads}$ is about 15, 10, 20 percent for Group I, II and III, respectively. The kind of ligand does not effect the $HO_{ads}$ to $H_2O_{ads}$ ratio, but reducing agent.

**Table 3.4.** O 1s core binding energies, eV, in all prepared catalysts and the relative intensities of species on catalyst surface.

| | O 1s | O 1s |
|---|---|---|
| Catalysts | $HO_{ads}$ | $H_2O_{ads}$ |
| Catalyst Ia | 531.2 (86.4) | 533.2 (13.6) |
| Catalyst Ib | 531.1 (84.3) | 533.0 (15.7) |
| Catalyst Ic | 531.5 (85.3) | 533.2 (14.7) |
| Catalyst IIa | 531.4 (90.8) | 533.2 (9.2) |
| Catalyst IIb | 531.5 (91.4) | 533.2 (8.6) |
| Catalyst IIc | 531.5 (91.2) | 533.2 (8.8) |
| Catalyst IIIa | 531.3 (81.9) | 533.2 (18.1) |
| Catalyst IIIb | 531.3 (79.8) | 533.2 (20.2) |
| Catalyst IIIc | 531.3 (78.4) | 533.2 (21.6) |

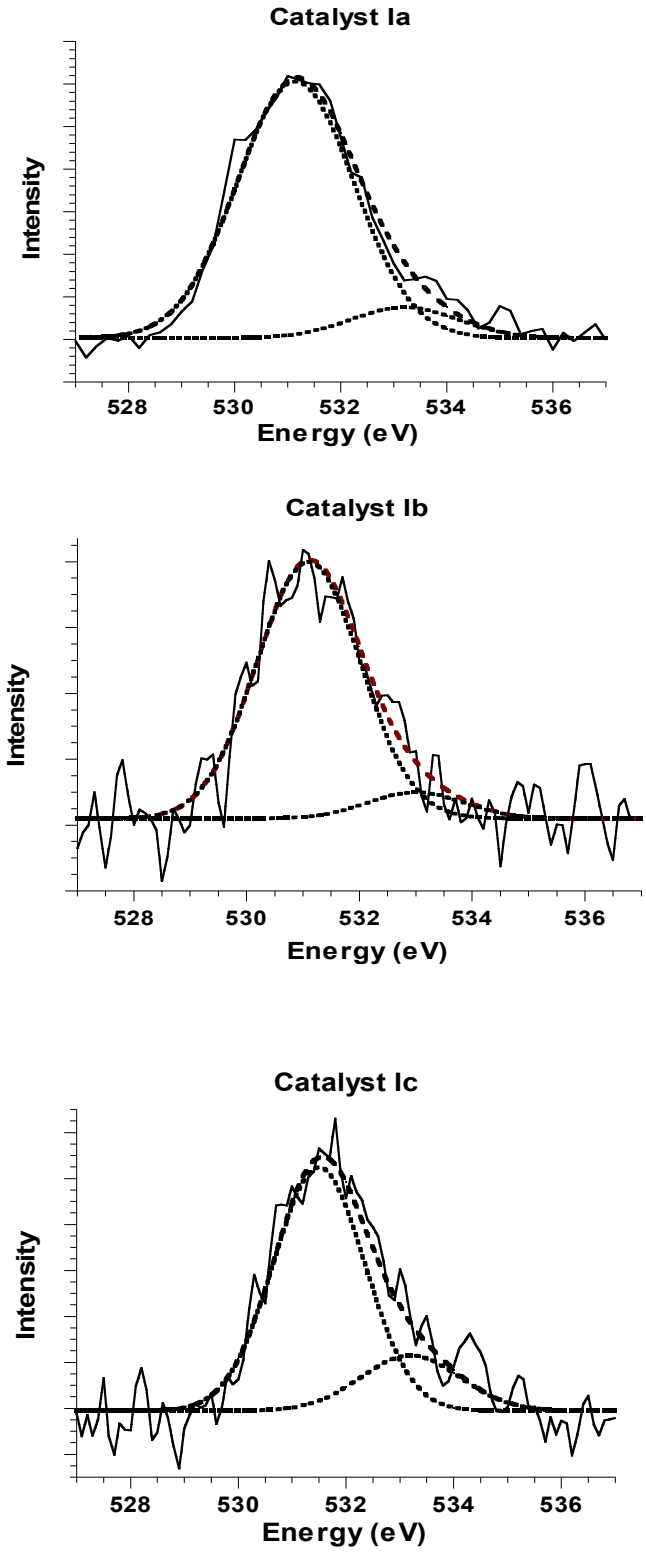


**Figure 3.7.a.** O 1s electron spectra of Catalyst Ia, Ib and Ic.

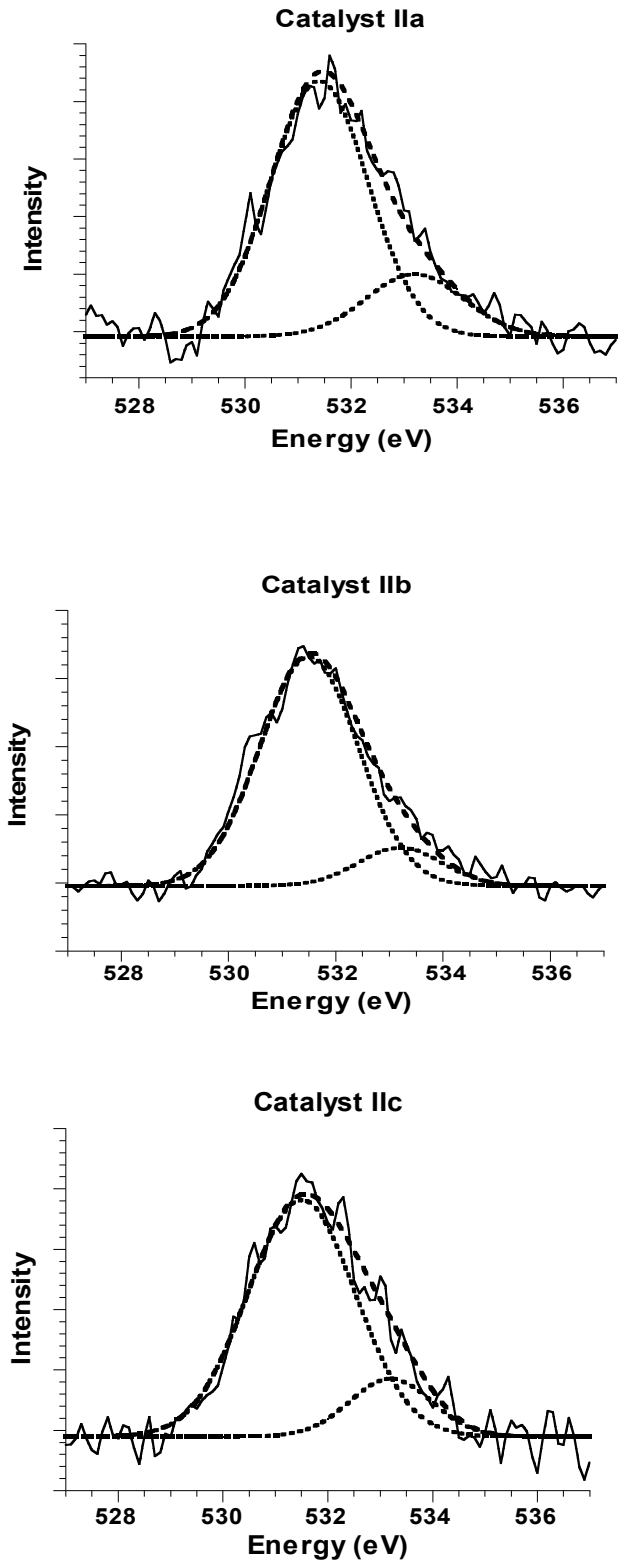


**Figure 3.7.b.** O 1s electron spectra of Catalyst IIa, IIb and IIc.

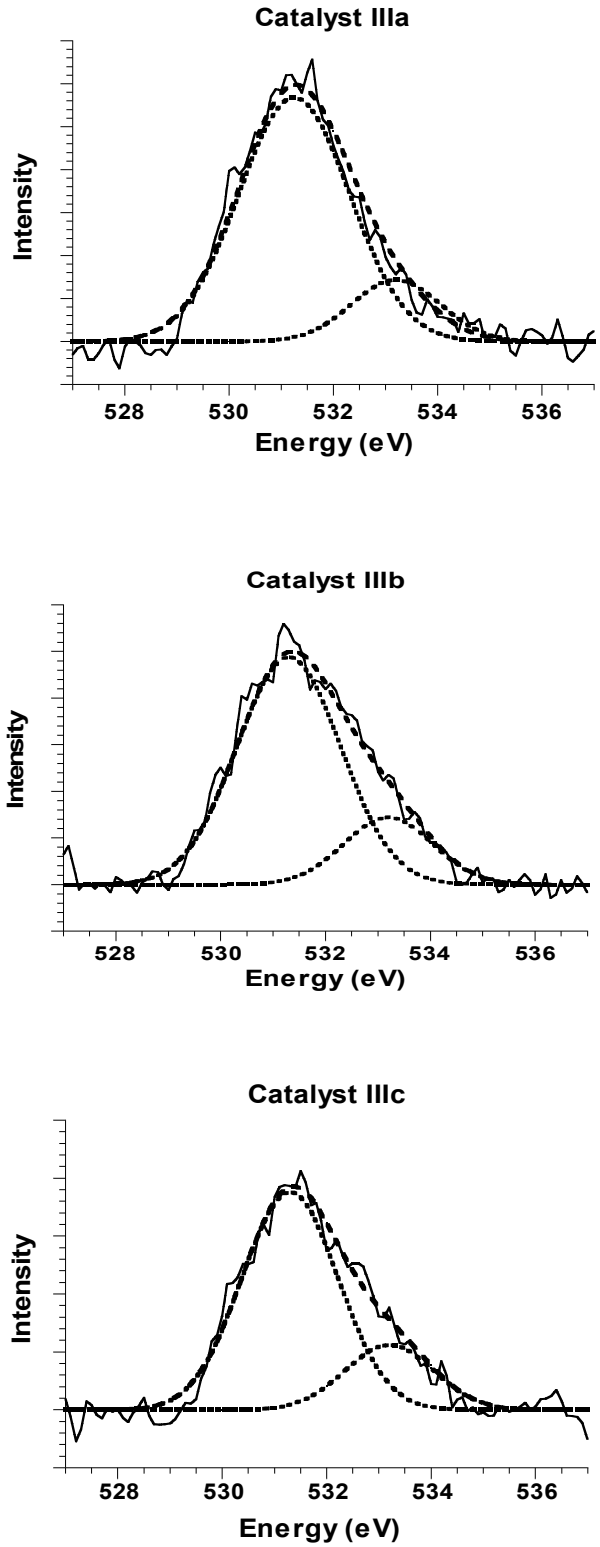


**Figure 3.7.c.** O 1s electron spectra of Catalyst IIIa, IIIb and IIIc.

## 3.5. CYCLIC VOLTAMMETRY

The cyclic voltammetry was used to evaluate electrochemical property and performance of all prepared catalysts towards methanol oxidation reaction. Each measurement was firstly recorded in electrolyte solution of 0.1 M $HClO_4$ at room temperature. Similar patterns were observed for all catalysts and a representative cyclic voltammogram was illustrated in Figure 3.8.a. The voltammograms consist of typical hydrogen and oxygen adsorption-desorption regions [5].

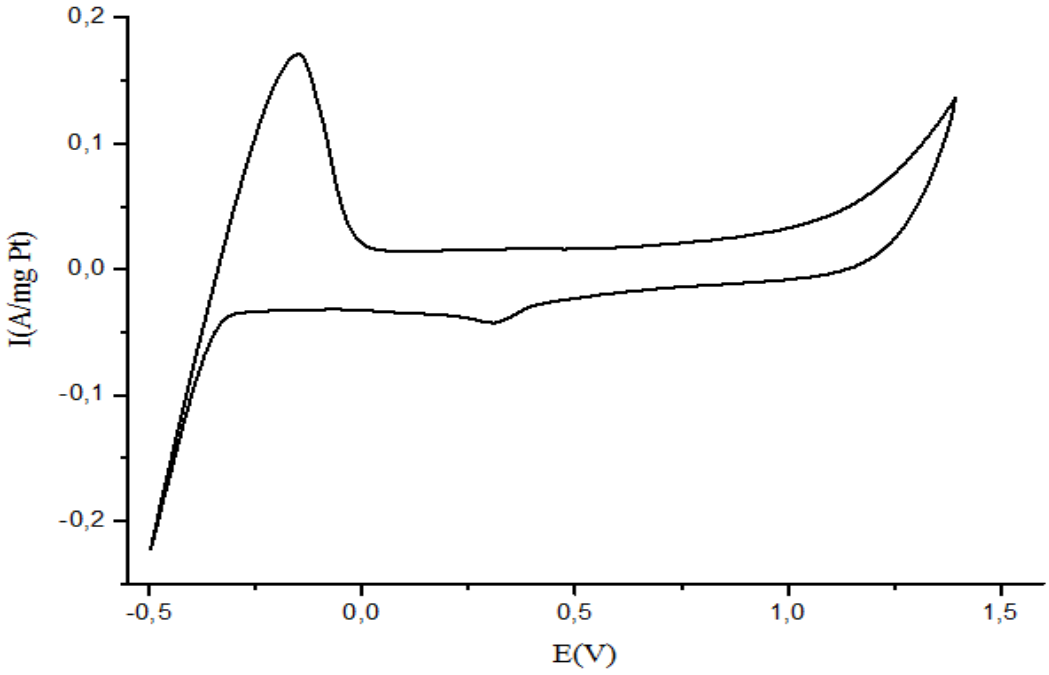


**Figure 3.8.a.** Cyclic voltammogram of Catalyst Ia in 0.1 M $HClO_4$ at room temperature.

The measurements were repeated after addition of methanol into 0.1 M $HClO_4$ electrolyte solution. The resulting cyclic voltammograms exhibited characteristic features of methanol oxidation reaction with forward and reverse anodic peaks. A typical cyclic voltammogram of methanol oxidation reaction is given in Figure 3.8.b. As can be seen from the figure, the electro-oxidation of methanol commences at

about 0.45 V and reach maximum at about 0.65 V in forward scan. In reverse scan, oxidation recommences around 0.5 - 0.6 V after intermediate carbon species on Pt surface were removed [30,34]. In order to evaluate the performance of the catalysts clearly, the only anodic part of the cyclic voltammogram was considered and given in Figure 3.9.a.b.c. and where the surfactants were kept constant while the reducing agents were changed. From these figures, it is possible to determine the order of performance of catalysts as Catalyst II < Catalyst I < Catalyst III, in which the most active catalysts were prepared by using formaldehyde as a reducing agent and the least active ones were prepared by hydrazine. The type of surfactant does not affect the order. In order to find the best catalyst, the most active catalysts from each Figure 3.9.a, b and c were chosen and a new Figure 3.9.d. were drawn. As can be seen from the figure, the best catalyst is Catalyst IIIb with an activity of 258 mA/mg Pt towards methanol oxidation reaction. When the activity of Catalyst IIIb was compared with previously reported catalyst, it was found that the performance of Catalyst IIIb is 3.5 times larger than commercial E-TEK 40% Pt/Vulcan XC-72 catalyst which has an activity of 75 mA/mg Pt towards methanol oxidation reaction [69]. The superior electrocatalytic performance of Group III catalyst towards methanol oxidation reaction can be attributed to different parameters such as active surface area, morphology of platinum nanoparticles and the amount of $H_2O_{ads}$ and $HO_{ads}$ on the surface of catalyst. Although the largest surface area from the BET analysis was observed for Group I catalyst (30 - 35 $m^2/g$), it did not show highest performance towards methanol oxidation reaction. This inconsistency can be explained by morphology or shape-dependent properties of catalysts rather than size. It is believed that the presence of cubic platinum nanoparticles, as in Group I catalyst, decrease the performance of catalysts. This idea was also supported by El-Sayed and co-workers. According to them, cubic-shaped Pt nanoparticles which are mainly composed of (100) interphase demonstrate the lowest activity compared to spherical and tetrahedral-shaped Pt nanoparticles involving mainly (111) interphase owing to different fraction of surface atoms located on corners and edges of Pt nanoparticles [70,71]. The activity of catalysts can also be associated with the adsorbed species on the surface of catalyst. Although the role of adsorbed water and hydroxides is not

fully understood in the mechanism of methanol oxidation reaction, it is believed that an increase in the amount of $H_2O_{ads}$ on the surface of catalyst causes an increase in the performance of catalyst towards methanol oxidation reaction. Similar result was obtained in the previous work [25].

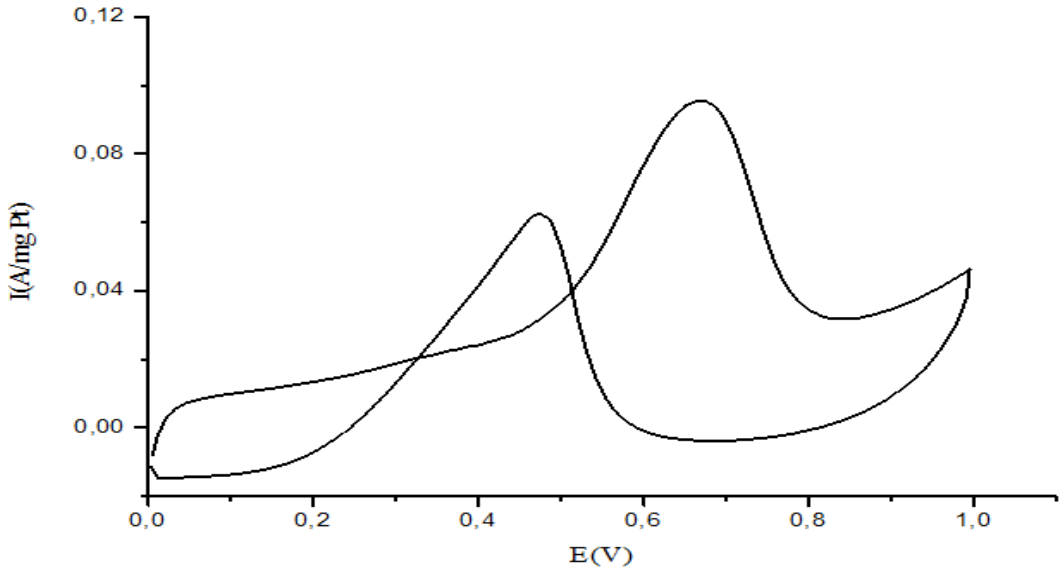


**Figure 3.8.b.** Cyclic voltammogram of Catalyst IIb in 0.1 M $HClO_4$ + 0.5 M $CH_3OH$ at room temperature.

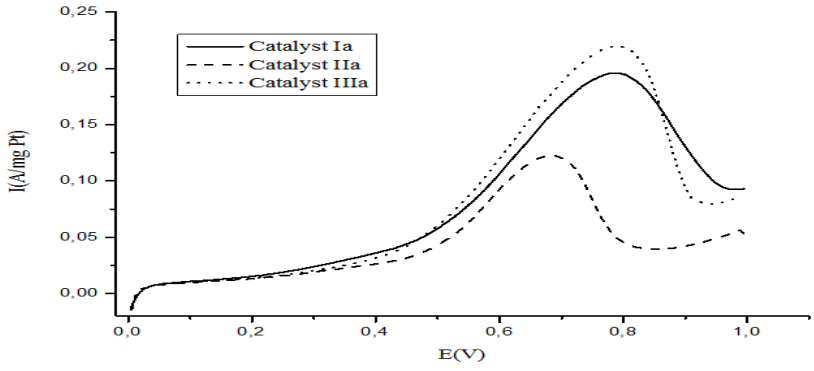


**Figure 3.9.a.** Cyclic voltammogram of Catalysts Ia, IIa, and IIIa in 0.1 M $HClO_4$ + 0.5 M $CH_3OH$ at room temperature.

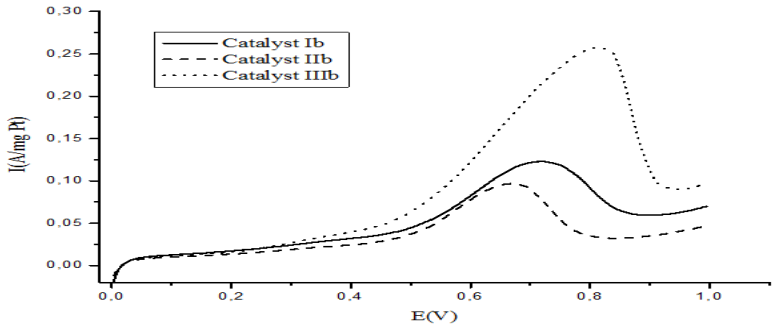


**Figure 3.9.b.** Cyclic voltammogram of Catalysts Ib, IIb and IIIb in 0.1 M $HClO_4$ + 0.5 M $CH_3OH$ at room temperature.

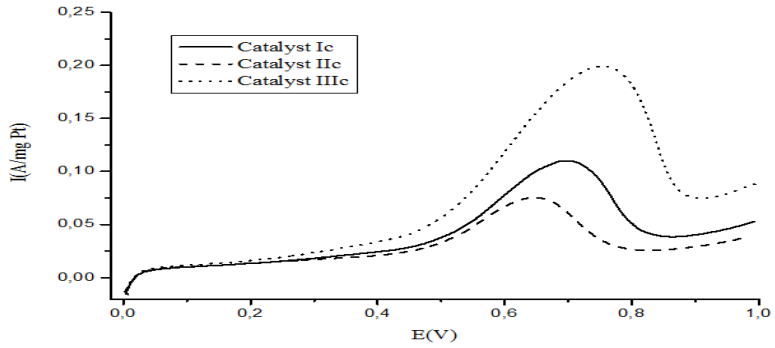


**Figure 3.9.c.** Cyclic voltammogram of Catalysts Ic, IIc and IIIc in 0.1 M $HClO_4$ + 0.5 M $CH_3OH$ at room temperature.

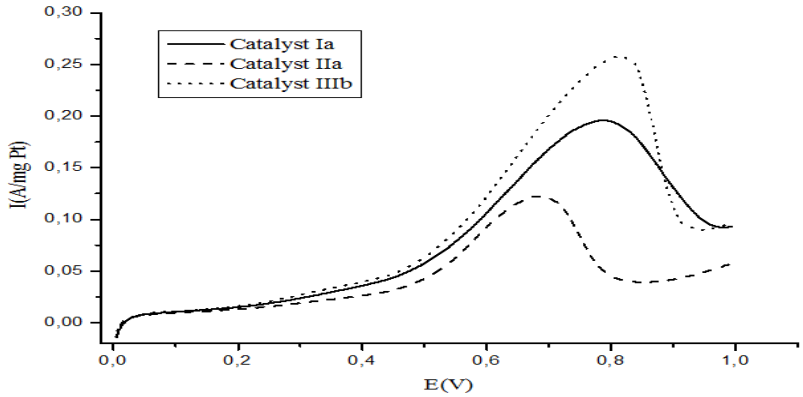


**Figure 3.9.d.** Cyclic voltammogram of Catalysts Ia, IIa and IIIb in 0.1 M $HClO_4$ + 0.5 M $CH_3OH$ at room temperature.

### 3.6. CHRONOAMPEROMETRY

The long-term stability of all prepared catalysts was determined by chronoamperometry (CA) under the same conditions. The methanol oxidation curves of all prepared catalysts were recorded as a function of time at the potential of 0.7 V for a period of 3600 s. The resulting CA curves were classified into three groups with respect to the same surfactant and demonstrated in Figure 3.10.a.b.c. As it can be seen from the figures, each oxidation curve exhibited a similar trend with a rapid current decay, which signals the poisoning of catalysts. Neverthless, at the end of 3600 s, the methanol oxidation curves have stabilized and shown an activity order of Group II < Group I < Group III towards methanol oxidation reaction. Accordingly, the Group III catalysts were detected as the most stable and poisoning-tolerance catalysts while the Group II catalysts were determined as the least stable ones. These results are in a good agreement with the cyclic voltammogram results.

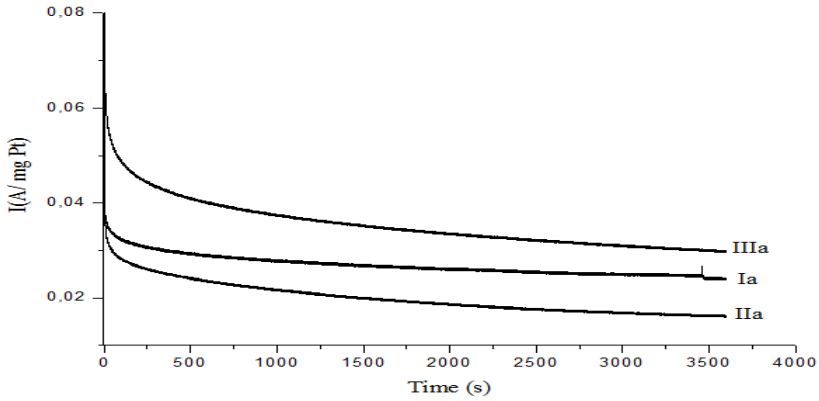


**Figure 3.10.a.** Chronoamperometric curves of methanol oxidation on Catalysts Ia, IIa and IIIa at 0.7 V in 0.1 M $HClO_4$ + 0.5 M $CH_3OH$ at room temperature.

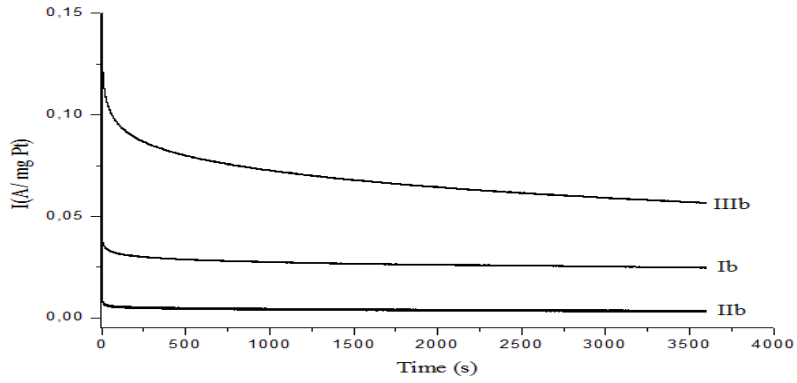


**Figure 3.10.b.** Chronoamperometric curves of methanol oxidation on Catalysts Ib, IIb and IIIb at 0.7 V in 0.1 M $HClO_4$ + 0.5 M $CH_3OH$ at room temperature.

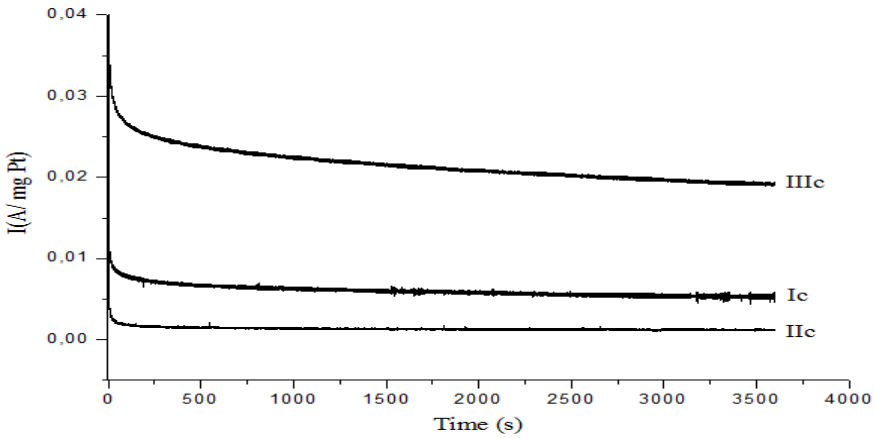


**Figure 3.10.c.** Chronoamperometric curves of methanol oxidation on Catalysts Ic, IIc and IIIc at 0.7 V in 0.1 M $HClO_4$ + 0.5 M $CH_3OH$ at room temperature.

# CHAPTER 4

# CONCLUSIONS

Carbon-supported platinum nanoparticle catalysts were prepared by using different reducing agents (sodium borohydride, hydrazine and formaldehyde) and surfactants (hexylamine, N-methylhexylamine and N,N-dimethylhexylamine), up to our knowledge last two were used for the first time. The physical, electrochemical characterization and the performance of the catalysts were conducted by XRD, TEM, XPS, CV, ICP, BET and CA and the following results were obtained:

i. Platinum crystallizes in face-centered cubic (fcc) structure and they have different size and morphology depending on the reducing agents used. Platinum nano (5 nm) and agglomerated (20 - 200 nm) particles were obtained in form of cubic, compact circular, less dense circular by $NaBH_4$, hydrazine and formaldehyde, respectively.

ii. The surface area of catalyst were found to be 30 - 35 $m^2/g$, 4 - 10 $m^2/g$ and 20 - 30 $m^2/g$ for Group I, II and III, respectively.

iii. Platinum was found to be in zero ( ~ 65 -71%) and +4 (~ 35 - 29%) oxidation states and peak positions did not change.

iv. The surface of catalysts were covered by $H_2O_{ads}$ and $HO_{ads}$ and their percentages were 10:90, 15:85 and 20:80 for Group II, Group I and Group III, respectively.

v. Catalyst IIIb was found to be the most active catalyst toward methanol oxidation reaction. It showed 3.5 times greater performace than commercial E-TEK Pt catalyst.

vi. Performance of the catalysts depends on

a) active surface area,
b) ratio of $H_2O_{ads}$ to $HO_{ads}$, and
c) morphology of catalysts.

# REFERENCES


[1] Li, X., *Principles of Fuel Cells,* Taylor & Francis Group, New York, 2006.

[2] Mitchell, W. Jr., *Fuel Cells,* Academic Press Inc., New York, 1963.

[3] Bagotsky, V.S., *Fuel Cells: Problems and Solutions*, John Wiley & Sons, Inc., New Jersey, 2009.

[4] Caretta, L., Friedrich, K.A., Stimming, U., *ChemPhysChem.,* 1, 162-193, 2000.

[5] Şen, S., Activity of Carbon Supported Platinum Nanoparticles Toward Methanol Oxidation Reactions: Role of Metal Presursor and New Surfactants, Master of Science Thesis in Chemistry, METU, Ankara, 2008.

[6] Gökağaç, G., Metal Oxides as Promoters for Methanol Oxidation, Doctor of Philosophy Thesis in Chemistry, University of Sydney, Australia, 1993a.

[7] Hart, A.B.,*Womack, G.J., Fuel Cells: Theory and Application*, Chapman & Hall (Ltd.), London, 1967.

[8] Milewski, J., Swirski, K., Santarelli, M., Leone, P., *Advanced Methods of Solid Oxide Fuel Cell Modelling,* Springer-Verlag, London, 2011.

[9] Hoogers, G., Section I, *Fuel Cell Technology Handbook*, CRS Press LLC, Florida, 2003.

[10] Şen, F., The Preparation and Analysis of New Carbon Supported Pt and Pt+Second Metal Nanoparticles Catalysts for Direct Methanol Fuel Cells, Doctor of Philosophy Thesis in Chemistry, METU, Ankara, 2012.

[11] Hogart, M.P., Hards, G.A., *Platinum Metals Rev.*, 40(4), 150-159, 1996.

[12] Guo, J.W., Zhao, T.S., Prabhuram, J., Wong, C.W., *Electrochim. Acta*., 50, 1973–1983, 2005.

[13] Horikoshi, S., Serpone, N., *Microwaves in Nanoparticle Synthesis: Fundamentals and Applications,* WILEY-VCH, Weinheim, 2013.

[14] Hosokawa,M., Nogi, K., Naito, M., Yokoyama, T., *Nanoparticle Technology Handbook*, Elsevier BV., Amsterdam, 2007.

[15] Wang, X., Li, C., Shi, G., *Phys. Chem. Chem. Phys.,* 16, 10142-10148, 2014.

[16] Guo, S., Wang, E., *Nano Today,* 6, 240-264, 2011.

[17] Li, W., Liang, C., Zhou, W., Qui, J., Zhou, Z., Sun, G., Xin, Q., *J. Phys. Chem. B,* 107, 6292-6299, 2003.

[18] Kadirgan, F., Beyhan, S., Atilan, T., *Int. J. Hydrogen Energy,* 34, 4312-4320, 2009.

[19] Huang, H., Wang, X., *J. Mater. Chem. A,* 2, 6266-6291, 2014.

[20] Öztürk, Z., Şen, F., Şen, S., Gökağaç, G., *J. Mater. Sci.,* 47, 8134-8144, 2012.

[21] Şen, F., Gökağaç, G., *Energy & Fuels,* 22, 1858-1864, 2008.

[22] Liu, Z., Ling, X.Y., Su, X., Lee, J.Y., *J. Phys. Chem. B,* 108, 8234-8240, 2004.

[23] Şen, S., Şen, F., Gökağaç, G., *Phys. Chem. Chem. Phys.,* 13, 6784-6792, 2011.

[24] Jiang, Q., Peng, Z., Xie, X., Du, K., Hu, G., Liu, Y., *Trans. Nonferrous Met. Soc. China,* 21, 127-132, 2011.

[25] Papp, S., Patakfalvi, R., Dekany, I., *Croat. Chem. Acta.,* 80 (3-4), 493-502, 2007.

[26] Ertan, S., Şen, F., Şen, S., Gökağaç, G., *J. Nanopart. Res.,* 14, 922-933, 2012.

[27] Yang, J., Lee, J. Y., Too, H.F., *Anal. Chim. Acta,* 571, 206-210, 2006.

[28] Cuenya, B.R., *Thin Solid Films,* 518, 3127-3150, 2010.

[29] Castro, E.G., Salvatierra, R.V., Schreiner, W.H., Oliveira, M.M., Zarbin, A.J.G., *Chem. Mater.,* 22, 360-370, 2010.

[30] Deivaraj, T.C., Chen, W., Lee, J.Y., *J. Mater. Chem.,* 13, 2555-2560, 2003.

[31] Şen, F., Gökağaç, G., *J. Phys. Chem. C,* 111, 5715-5720, 2007.

[32] Şen, F., Şen, S., Gökağaç, G., *Phys. Chem. Chem. Phys,.* 13, 1676-1684, 2011.

[33] Şen, F., Gökağaç, G., Şen, S., *J. Nanopart. Res.*15, 1979-1988, 2013.

[34] Şen, F., Gökağaç, G., *J. Appl. Electrochem.,* 44, 199-207, 2014.

[35] Gökağaç, G., Leger, J.M., Hahn, F., *Z. Naturforsch,* 56 b, 1306, 2001.

[36] Kissinger, P.T., Heineman, W.R., *Laboratory Techniques in Electroanalytical Chemistry*, *2nd Ed.*, Marcel Dekker, Inc., New York, 1996.

[37] Öztürk, Z., Carbon Supported Platinum-Palladium Catalysts for Methanol and Ethanol Oxidation Reactions, Master of Science Thesis in Chemistry, METU, Ankara, 2011.

[38] Evans, D.H., O'Connell, K.M., Petersen R.A., Kelly M.J. *J. Chem. Educ.*, 60(4), 290-293, 1983.

[39] Scholz, F., *Electroanalytic Methods: Guide to Experiments and Applications*, Springer-Verlag, Heidelberg, 2010.

[40] Avcı, E., An Electrochemical Study of the Deposition of Copper and Silver on Thymine Modified Au(111), Doctor of Philosophy Thesis, Free University of Berlin, Berlin, Germany, 2007.

[41] Brundle, C.R., Evans, C.A., Wilson, S., *Encyclopedia of Materials Characterization: Surfaces, Interfaces, Thin Films,* Elsevier Butterworth-Heinemann, Boston, 1992.

[42] Cao, G., Wang, Y., *Nanostructures and Nanomaterials: Synthesis, Properties, and Applications,* World Scientific Publishing, Singapore, 2011.

[43] Chung, F.H., Smith, D.K., *Industrial Applications of X-Ray Diffraction,* Marcel Dekker, Inc., New York, 2000.

[44] Suryanarayana, C., Norton, M.G., *X-Ray Diffraction: A Practical Approach,* Plenum Press, New York, 1998.

[45] Klug, H., Alexander, L., *X-ray diffraction procedures*, *1st Ed*., John Wiley & Sons, Inc., New York, 1954.

[46] Hutchison, J., Kirkland, A., *Nanocharacterisation,* RSC Publishing, Cambridge, 2007.

[47] Williams, D.B., Carter, C.B., *Transmission Electron Microscopy: A Textbook for Materials Science,* Springer, New York, 2009.

[48] Egerton, R.F., *Physical Principles of Electron Microscopy: An Intoduction to TEM, SEM, and AEM*, Springer Science+Business Media, Inc., NewYork, 2005.

[49] Reimer, L., Kohl, H., *Transmission Electron Microscopy: Physics of Image Formation,* Springer, New York, 2008.

[50] Barron, A.R., *Physical Methods in Chemistry and Nano Science,* Connexions, Houston, 2012.

[51] Muilenberg, G.E., *Handbook of X-Ray Photoelectron Spectroscopy,* Perkin-Elmer Corp., Minnesota, 1979.

[52] Watts, J.F., Wolstenholme, J., *An Introduction to Surface Analysis by XPS and AES*, John Wiley and Sons, Ltd., Chichester, 2003.

[53] Skoog, D. A., Holler F. J., Crouch S.R., *Principles of Instrumental Analysis*, Thomson Brooks/Cole, Canada, 2007.

[54] Lowell, S., Shields, J.E., *Powder Surface Area and Porosity,* Chapman & Hall, London, 1991.

[55] Stanley-Wood, N., Lines, R. W., *Particle Size Analysis,* Royal Society of Chemistry, UK, 1992.

[56] Branuer, S., Emmett, P. H., Teller, E., *J. Amer. Chem. Soc.,* 60, 309-319, 1938.

[57] Condon, J.B., *Surface Area and Porosity Determinations by Physisorption: Measurements and Theory,* Elsevier, Amsterdam, 2006.

[58] Griffiths, P., de Hasseth, J.A., *Fourier Transform Infrared Spectrometr*y, Wiley-Blackwell, 2007.

[59] Sun, D., *Infrared Spectroscopy for Food Quality Analysis and Control,* Elsevier Inc., New York, 2009.

[60] Mizikoshi, Y., Takagi, E., Okuno, H., Oshima, R., Maeda, Y., Nagata, Y., *Ultrason Sonochem.,* 8, 1-6, 2001.

[61] Yang, J., Deivaraj, T.C., Too, H.P., Lee, J.Y., *J. Phys. Chem. B*, 108, 2181-2185, 2004.

[62] Yang, J., Lee, J.Y., Deivaraj, T.C., Too, H.P., *J. Colloid Interf. Sci.*, 277, 95-99, 2004.

[63] Yang, J., Lee, J.Y., Deivaraj, T.C., Too, H.P., *Colloid Surface A:Physicochem. Eng. Aspects,*, 240, 131-134, 2004.

[64] Yonezawa, T.,Toshima, N., Wakai, C., Nakahara M., Nishinaka, M., Tominaga, T., Nomura, H., *Colloids Surf.A,* 169, 35-45, 2000.

[65] Liang, L., Sun, G., Sun, S., Liu J., Tang, S., Li, H., Zhou, B., Xin, Q., *Electrochim. Acta.,* 50, 5384-5389, 2005.

[66] Liu, Z., Lee, J.Y., Han, M., Chen, W., Gan, L.M., *J. Mater. Chem.,* 12, 2453-2458, 2002.

[67] Peuckert, M.,*Electrochim. Acta.,* 29(10), 1315-1320, 1984.

[68] Peuckert, M., Bonzel, H.P., *Surf. Sci.*, 145, 239-259, 1984.

[69] Şen, F., Gökağaç, G., *J. Phys. Chem. C,* 111, 1467-1473, 2007

[70] Zhou, M., Xiao, P., Guo, W., Deng, J., Liu, F., Zhang, Y., *J. Electrochem. Soc.* 161(3), 133-137, 2014.

[71] Narayanan, R.,Shape-dependent Nanocatalysis and The Effect of Catalysis on the Shape and Size of Colloidal Metal Nanoparticles, Doctor of Philosophy Thesis in Chemistry, Georgia Institue of Technology, Atlanta, 2005.